nature chemical biology

Article

https://doi.org/10.1038/s41589-023-01279-5

Sniper2L is a high-fidelity Cas9 variant with high activity

Received: 11 May 2022

Accepted: 2 February 2023

Published online: 9 March 2023

Check for updates

Young-hoon Kim[1,2,3,4,20], Nahye Kim[2,5,20], Ikenna Okafor[6,20], Sungchul Choi[2], Seonwoo Min[7], Joonsun Lee[1], Seung-Min Bae[1], Keunwoo Choi[1], Janice Choi[8], Vinayak Harihar[8], Youngho Kim[1], Jin-Soo Kim[9], Benjamin P. Kleinstiver[10,11,12], Jungjoon K. Lee[1], Taekjip Ha[8,13,14,15] & Hyongbum Henry Kim[2,4,5,16,17,18,19]

Although several high-fidelity SpCas9 variants have been reported, it has been observed that this increased specificity is associated with reduced on-target activity, limiting the applications of the high-fidelity variants when efficient genome editing is required. Here, we developed an improved version of Sniper–Cas9, Sniper2L, which represents an exception to this trade-off trend as it showed higher specificity with retained high activity. We evaluated Sniper2L activities at a large number of target sequences and developed DeepSniper, a deep learning model that can predict the activity of Sniper2L. We also confirmed that Sniper2L can induce highly efficient and specific editing at a large number of target sequences when it is delivered as a ribonucleoprotein complex. Mechanically, the high specificity of Sniper2L originates from its superior ability to avoid unwinding a target DNA containing even a single mismatch. We envision that Sniper2L will be useful when efficient and specific genome editing is required.

Applications of SpCas9-induced genome editing are often restricted due to off-target effects or insufficient on-target editing. Several high-fidelity variants, such as eSpCas9(1.1)[1], Cas9–HF1[2], HypaCas9[3], Cas9_R63A/Q768A[4], evoCas9[5], HiFi Cas9[6] and Sniper–Cas9 (referred to in this manuscript as Sniper1)[7], have been developed. However, the modifications introduced in these variants to decrease off-target cleavage also hamper their general on-target cleavage activities, such that a trade-off between the general activity and specificity[8] is observed when the variants are tested with a large number of target sequences. A high-fidelity variant that exhibits a general activity level similar to that of SpCas9 would facilitate applications of SpCas9-based genome editing in areas including gene therapy and genetic screening.

In this study, we developed Sniper2L, a next-generation high-fidelity variant, using directed evolution of Sniper1. To evaluate

[1]Toolgen, Seoul, Republic of Korea. [2]Department of Pharmacology, Yonsei University College of Medicine, Seoul, Republic of Korea. [3]Graduate Program of Biomedical Engineering, Yonsei University College of Medicine, Seoul, Republic of Korea. [4]Graduate Program of NanoScience and Technology, Yonsei University, Seoul, Republic of Korea. [5]Graduate School of Medical Science, Brain Korea 21 Project, Yonsei University College of Medicine, Seoul, Republic of Korea. [6]Department of Biology, Johns Hopkins University, Baltimore, MD, USA. [7]LG AI Research, Seoul, Republic of Korea. [8]Department of Biophysics, Johns Hopkins University, Baltimore, MD, USA. [9]Department of Biochemistry and NUS Synthetic Biology for Clinical & Technological Innovation (SynCTI), National University of Singapore, Singapore, Singapore. [10]Center for Genomic Medicine, Massachusetts General Hospital, Boston, MA, USA. [11]Department of Pathology, Massachusetts General Hospital, Boston, MA, USA. [12]Department of Pathology, Harvard Medical School, Boston, MA, USA. [13]Department of Biophysics and Biophysical Chemistry, Johns Hopkins University, Baltimore, MD, USA. [14]Department of Biomedical Engineering, Johns Hopkins University, Baltimore, MD, USA. [15]Howard Hughes Medical Institute, Baltimore, MD, USA. [16]Center for Nanomedicine, Institute for Basic Science, Seoul, Republic of Korea. [17]Yonsei–Institute for Basic Science Institute, Yonsei University, Seoul, Republic of Korea. [18]Severance Biomedical Science Institute, Yonsei University College of Medicine, Seoul, Republic of Korea. [19]Institute for Immunology and Immunological Diseases, Yonsei University College of Medicine, Seoul, Republic of Korea. [20]These authors contributed equally: Young-hoon Kim, Nahye Kim, Ikenna Okafor. e-mail: jj.lee@toolgen.com; tjha@jhu.edu; hkim1@yuhs.ac

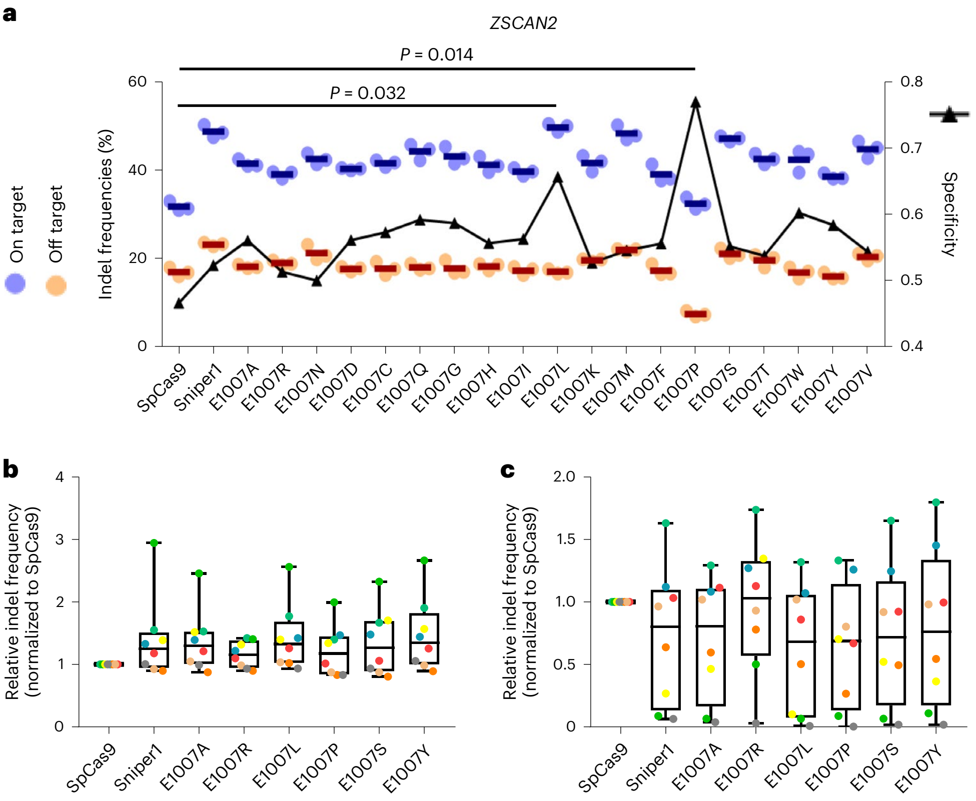

Fig. 1 | Schematics for hit identification using Sniper screen and hit optimization using site saturation mutagenesis. a, Indel frequencies at on-target (blue) and off-target (orange) sequences and specificities determined after transfection of plasmids encoding SpCas9 or Sniper1 variants into HEK293T cells. Sniper1 variants were generated by site saturation mutagenesis at the 1,007th amino acid codon (originally a Glu codon); the resulting amino acids at that position are shown on the *x* axis. Indel frequencies and specificities are shown on the left and right *y* axes, respectively. Specificity was calculated as 1 − (indel frequencies at off-target sequences divided by those at on-target sequences). The averages of three replicates are indicated by dark blue and red horizontal lines. The name of the gene in which the target sequence is located is indicated at the top of the graph. The number of independent transfections (*n*) is *n* = 3. Statistical significances are shown (no statistical significance ($P > 0.05$) unless specified in the figure; Kruskal–Wallis test). **b**,**c**, Indel frequencies induced by SpCas9 and Sniper1 variants based on plasmid delivery at on-target (**b**) and off-target (**c**) sequences in HEK293T cells. The results for each target sequence are shown in Supplementary Fig. 5. The boxes represent the 25th, 50th and 75th percentiles; whiskers show the 10th and 90th percentiles. The number of analyzed target sequences *n* = 8.

the specificity and activity of Sniper2L at a large number of target sequences, we delivered it together with guide RNA (gRNA) using two different methods: lentiviral expression and electroporation of ribonucleoprotein (RNP) complexes, a therapeutically relevant method. Our high-throughput evaluations showed that Sniper2L exhibits higher fidelity than Sniper1 while retaining its general level of activity, similar to that of SpCas9, overcoming the trade-off between activity and specificity regardless of the delivery method. We believe that Sniper2L will facilitate applications of genome editing due to its high general activity and low levels of off-target effects.

Results

Directed evolution of Sniper1

Previously, we used 'Sniper screen' for directed evolution of SpCas9 in *Escherichia coli* (*E. coli*)[7] (Supplementary Fig. 1). In brief, both positive (SpCas9-mediated cleavage of a plasmid containing a lethal gene (*ccdB*)) and negative (lack of *E. coli*-killing cleavage at a mismatched off-target genomic site) selection pressure were applied to SpCas9 mutant libraries, in which the entire SpCas9-encoding sequence contained random errors (library complexity, up to 10^7); a fragment of the human *EMX1* gene was used for the matched and mismatched target sequences. The initial Sniper screen resulted in the identification of three SpCas9 variants named Clone-1, Clone-2 and Clone-3 (ref. [7]). We selected Clone-1 (that is, Sniper1) because it induced high frequencies of on-target indels with many different single-guide RNAs (sgRNAs) compared with Clone-2 and Clone-3, which showed low on-target indel efficiencies with the same sgRNAs. High indel frequencies were observed when these variants were tested with the sgRNA EMX1.3, which was used in the Sniper screen. To distinguish SpCas9 variants with reduced on-target activities, such as Clone-2 and Clone-3, from those with maintained on-target activities, we needed to perform the Sniper screen with an sgRNA that would result in low on-target indel efficiencies with Clone-2 and Clone-3 while retaining wild-type (WT)-level indel efficiencies with Clone-1. When we used EMX1.6 sgRNA, which was previously used to determine the specificity of SpCas9 (ref. [9]), we found that the on-target activities of Clone-2 and Clone-3 were dramatically decreased as compared with that of Clone-1 (Supplementary Fig. 2). Thus, we chose EMX1.6 sgRNA for screening in the current study. Because the mismatches in the previous Sniper screen were at positions 5–7 (proximal to the PAM) and positions 17 and 18 (distal to the PAM), we attempted to make a mismatch in the previously untested middle region, which spans positions 8–16. The center of the middle region would include positions 11–13 or 10–14. Among these positions, a previous study showed that the induction of C to U mutations at position 13 of an EMX1.6 sgRNA resulted in the highest relative cleavage efficiency[9]. In addition, this mismatch induces wobble base pairing, which generally results in high relative activities at mismatched targets (that is, low specificity) by SpCas9 and its variants[8]. Thus, as the sgRNA and

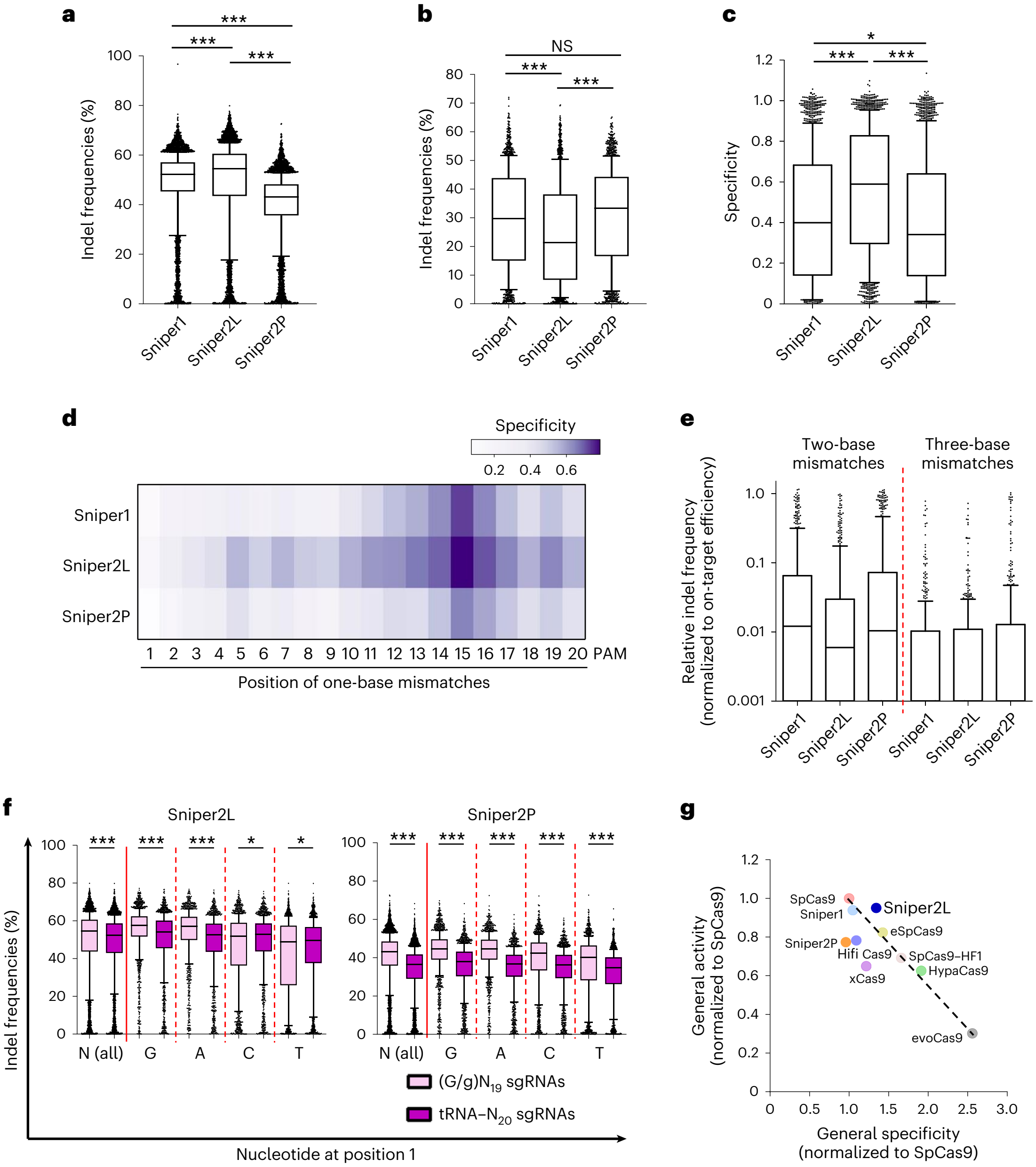

Fig. 2 | Comparison of Sniper1 variants. a, Indel frequencies at target sequences containing NGG PAMs. The number of target sequences (n) is $n = 7{,}702$. ***$P = 1.3 \times 10^{-35}$, $<1.3 \times 10^{-35}$ and $<1.3 \times 10^{-35}$ for the comparisons between Sniper1 and Sniper2L, between Sniper1 and Sniper2P, and between Sniper2L and Sniper2P, respectively; Kruskal–Wallis test. **a**–**c** and **f**, The boxes represent the 25th, 50th and 75th percentiles; whiskers show the 10th and 90th percentiles. **b**, Indel frequencies at target sequences with single-base mismatches containing NGG PAMs. The number of target sequences (n) is $n = 1{,}732$. NS, no statistically significant difference. ***$P = 3.2 \times 10^{-18}$ between Sniper1 and Sniper2L and $P = 8.6 \times 10^{-28}$ between Sniper2L and Sniper2P; Kruskal–Wallis test. **c**, General specificity of variants. Specificity was calculated as 1 − (indel frequencies at target sequences that harbor a single mismatch divided by those at perfectly matched target sequences). The number of target sequences (n) is $n = 1{,}734$, 1,732 and 1,734 for Sniper1, Sniper2L and Sniper2P, respectively. *$P = 0.15$ for the comparison between Sniper1 and Sniper2P, two-sided Mann–Whitney U test; ***$P = 4.08 \times 10^{-32}$ for the comparison between Sniper1 and Sniper2L, two-sided Mann–Whitney U test; ***$P = < 1.3 \times 10^{-35}$ for the comparison between Sniper2L and Sniper2P, two-sided Mann–Whitney U test. **d**, Specificity of variants depending on the mismatch position (details are in Supplementary Fig. 10). **e**, Relative indel frequencies analyzed at target sequences with consecutive two- or three-base transversion mismatches. The number of target sequences (n) is $n = 554$ and 531 for two- and three-base mismatches, respectively. **f**, Activity assessments at target sequences with (G/g)N$_{19}$ or tRNA–N$_{20}$ sgRNAs. The number of target sequences (n) is $n = 6{,}321$ (N), 1,666 (G), 1,467 (A), 1,626 (C) and 1, 562 (T) for Sniper2L and $n = 6{,}765$ (N), 1,807, 1,587, 1,721 and 1,650 (T) for Sniper2P. *P and ***$P = 8.39 \times 10^{-20}$ (N), 5.06×10^{-26} (G), 7.56×10^{-34} (A), 0.012 (C) and 0.04 (T) for Sniper2L and ***$P = 7.56 \times 10^{-34}$ (N) and $<1.3 \times 10^{-35}$ (G, A, C and T) for Sniper2P; two-sided Mann–Whitney U test. **g**, Relationship between the specificity and activity of SpCas9 and SpCas9 variants. Sniper2L represents an outlier of the general trade-off. The specificity and activity of the high-fidelity variants were taken from our previous study[8]. The dashed line shows the general trade-off relationship. NS, not significant.

mismatched target sequence pair, we used a gcgccacUgguugaugugau sgRNA and a gcgccacCggttgatgtgat mismatched target sequence (the mismatch at position 13 is capitalized).

Libraries encoding mutant versions of Sniper1 with random errors in the Sniper1 sequence were constructed using the three different mutagenesis kits that were used in the previous Sniper screen[7].

The Sniper-screen selection procedure was repeated four times with the EMX1.6 sgRNA (Supplementary Fig. 3). The final clones were sequenced, and a hotspot at the 1,007th amino acid of Sniper1 was identified (Supplementary Fig. 4). We introduced all possible amino acid mutations at the 1,007th amino acid position and measured the activities of these 19 variants at matched and mismatched target sequences using another three sgRNAs, which did not include EMX1.6 (Supplementary Table 1). Among the 19 variants, only E1007L and E1007P, but none of the remaining 17 variants, showed high on-target activity, high specificity and low off-target activity with at least two sgRNAs (Fig. 1a and Extended Data Fig. 1a,b). We randomly selected 4 variants of the remaining 17; these four variants displayed a wide range of average specificities when three sgRNAs were tested (Extended Data Fig. 1c). We evaluated the four variants together with the E1007L and E100P variants when targeted to a total of eight different sequences. We found that the ranks of the average specificities of the six selected variants for the three target sites were comparable with those for the eight target sites (Extended Data Figs. 1c and 2a). Importantly, we confirmed that only the E1007L and E1007P variants frequently showed high on-target activity and low off-target effects (Fig. 1b,c, Extended Data Fig. 2b–i and Supplementary Table 1). We named the E1007L and E1007P variants Sniper2L and Sniper2P, respectively, and used them for subsequent studies.

The activities and specificities of the Sniper2 variants

Although we compared Sniper2L and Sniper2P activities at eight target sequences, we cannot yet draw conclusions about the general activities of these two variants, which require an analysis of many more target sequences[8]. To evaluate the activities of these two variants at a large number of target sequences, we adopted a high-throughput evaluation approach that we previously used to compare the activities of various SpCas9 variants[8] in human embryonic kidney 293 T (HEK293T) cells (Extended Data Fig. 3a). For these high-throughput evaluations, we first generated individual cell lines, each containing a single copy of a variant-expressing lentivirus[8], which led to comparable expression levels of Sniper1 and the Sniper2 variants (Extended Data Fig. 3b). We then transduced our previously described lentiviral libraries of pairs of sgRNA-encoding and corresponding target sequences[8,10] into the Sniper1 variant-expressing cells and determined indel frequencies at the integrated target sequences by deep sequencing 4 and 7 days after the transduction of lentiviral libraries (Methods). The libraries used in these analyses, named A, B and C[8], contained 11,802, 23,679 and 7,567 sgRNA–target pairs, respectively. In brief, library A included 8,130 and 3,672 pairs to evaluate protospacer adjacent motif (PAM) compatibility and mismatch tolerance, respectively (Supplementary Dataset 1). Library B, which contained 8,744, 12,093 and 2,660 pairs with NGG (N = A, C, G or T), NGH (H = A, C or T) and non-NG PAMs, respectively, was used for validating variant activities at a large number of target sequences (Supplementary Dataset 1). In contrast to libraries A and B, in which the 5′ nucleotide in the sgRNA is always a G and thus, often mismatched with the target sequence (see below), library C utilized perfectly matched N_{20} sgRNAs generated by transfer RNA (tRNA)-associated processing (hereafter, tRNA–N_{20} sgRNAs), with the majority of target sequences taken from library B (Supplementary Dataset 1). Because indel frequencies between two technical replicates were well correlated (Supplementary Fig. 5), we combined the read counts from two replicates to draw more accurate conclusions[8].

We first determined the PAM compatibilities of the Sniper2 variants using library A, which contains target sequences with NNNN PAMs. We found that the PAM compatibilities of the Sniper1 variants were identical and that the highest average activities were observed at target sequences with NGG PAMs (Extended Data Fig. 4). These results are in line with the PAM compatibilities of other high-fidelity variants[8] and would be attributable to the lack of mutations within the PAM-interacting domain of the Sniper1 variants. Based on these results, target sequences with NGG PAMs were chosen for subsequent analysis.

We then evaluated the activities of the Sniper2 variants at a large number of matched and mismatched target sequences. For assessing on-target activities, the 8,744 target sequences with NGG PAMs in library B were utilized. We found that Sniper2L exhibited significantly higher efficiencies than Sniper1, whereas Sniper2P induced the lowest indel frequencies (Fig. 2a).

Next, we compared the specificities of the Sniper1 variants with that of Sniper1 by comparing activities at mismatched target sequences using library A. Given that a comparison of activities at mismatched target sequences can be biased when the activities at matched target sequences are substantially different between the comparison groups, we used 30 sgRNAs that induced comparable Sniper1 variant-directed indel frequencies either 4 or 7 days after transduction (Supplementary Fig. 6). Each of the 30 sgRNAs was paired with 98 target sequences harboring one-, two- or three-base mismatches (Methods). The activities of Sniper2L at the mismatched target sequences were significantly lower than those of Sniper1 and Sniper2P (Fig. 2b). If we define specificity as 1 − (indel frequencies at target sequences that harbor a single mismatch divided by those at perfectly matched target sequences)[8], the specificity of Sniper2L was significantly higher than that of Sniper2P and Sniper1 (Fig. 2c).

When we determined the specificity as a function of the mismatch position, we found that all three Sniper1 variants showed higher specificity in the PAM-proximal region as compared with the PAM-distal region (Fig. 2d and Supplementary Fig. 7). Similar higher specificities in the PAM-proximal region were also previously observed for other high-fidelity SpCas9 variants[8]. Notably, Sniper2L was less likely to tolerate mismatches in both the PAM-distal and -proximal regions as compared with Sniper1 and Sniper2P; in those regions, local specificity was highest at positions 5 and 15, respectively, which is compatible with the results of most previously reported high-fidelity variants[8].

Furthermore, all Sniper variants tolerated single-base wobble mismatches more than single-base transversion mismatches (Extended Data Fig. 5), which is in line with results from previous studies of SpCas9 variants[8,11]. The relative indel frequencies at mismatched target sequences containing two- or three-base transversion mismatches were dramatically reduced (Fig. 2e and Supplementary Fig. 8). Based on these results, we selected Sniper2L as our new version of Sniper1.

Because perfectly matched sgRNAs generated by the tRNA-associated processing system could increase the activity of some high-fidelity variants, such as eSpCas9(1.1), SpCas9–HF1 and evoCas9, but not HypaCas9 or xCas9 (refs. [8,12,13]), we compared the activities of the Sniper variants using library C, based on tRNA–N_{20} sgRNAs that perfectly match the targets, and library B, based on (G/g)N_{19} sgRNAs (hereafter, 20-nt guide sequences with a matched or mismatched 5′ guanosine are described as GN_{19} and gN_{19}, respectively). Such (G/g)N_{19} sgRNAs are expressed from a U6 promoter with a G at the 5′ terminus, which is often mismatched with the corresponding nucleotide (position 1) in the target sequence. We observed that Sniper2L and Sniper2P displayed slightly higher general activities with (G/g)N_{19} sgRNAs than with tRNA–N_{20} sgRNAs, although tRNA–N_{20} sgRNAs resulted in slightly higher Sniper2L-induced activities than did gN_{19} sgRNAs at target sequences starting with 5′ C or T (Fig. 2f).

Sniper2L shows improved specificity and high activity

We previously observed a trade-off between the general activity and specificity of SpCas9 variants[8]; when a high-fidelity variant displayed high fidelity or specificity, it also exhibited relatively low general activity. To examine whether the Sniper2 variants followed this trend, we measured their activity and specificity using eight sgRNAs that were previously used in the analysis of the other high-fidelity variants. We observed that Sniper2L displayed both enhanced fidelity and higher on-target activities compared with Sniper1. To our knowledge, Sniper2L

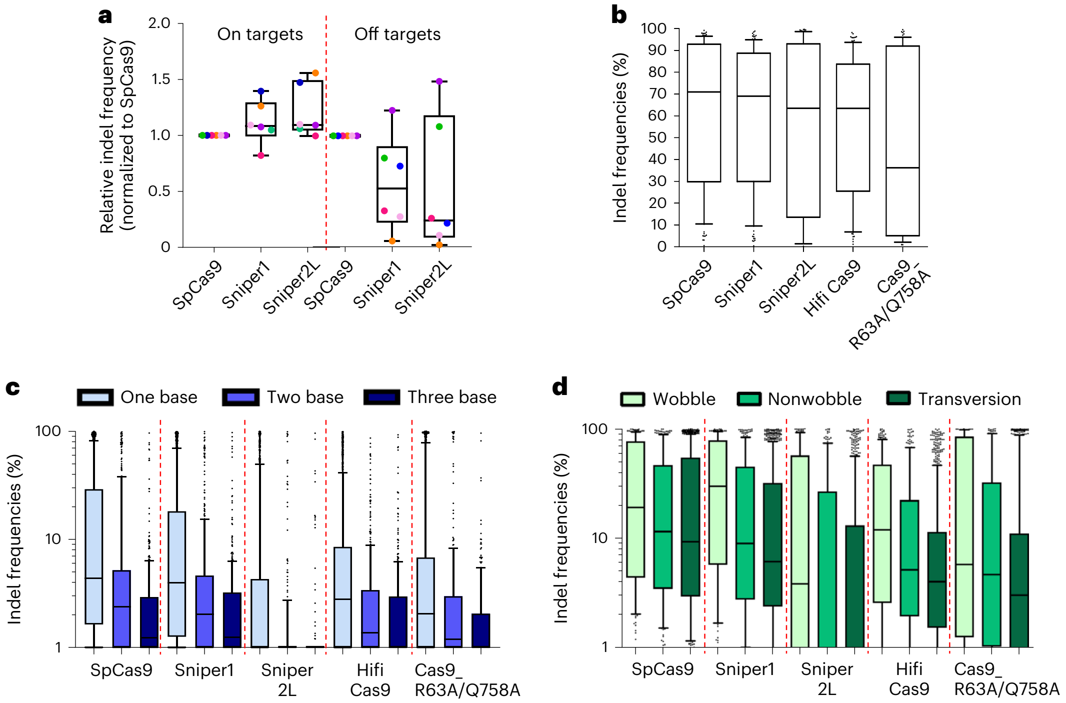

Fig. 3 | High-throughput evaluation of the activities of SpCas9 variants when delivered as RNPs. a, Indel frequencies induced by SpCas9 and Sniper1 variants delivered using a preassembled RNP format at matched and mismatched target sequences in HEK293T cells. Each dot represents the average value measured at each target; the six target sequences are distinguished using different colors. **a**–**d**, The boxes represent the 25th, 50th and 75th percentiles; the whiskers show the 10th and 90th percentiles. The number of analyzed target sequences (*n*) is *n* = 6. **b**, Indel frequencies at perfectly matched target sequences with NGG PAMs. The number of analyzed target sequences (*n*) is *n* = 105, 113, 81, 113 and 69 for SpCas9, Sniper1, Sniper2L, HiFi Cas9 and Cas9_R63A/Q768A, respectively. No statistically significant difference; Kruskal–Wallis test. **c**, Effects of the number of mismatches between the sgRNA and target sequence. The number of analyzed target sequences (*n*) is *n* = 2,236 (one base), 448 (two base) and 414 (three base) for SpCas9; *n* = 2,352, 446 and 296 for Sniper1; *n* = 1,641, 322 and 296 for Sniper2L; *n* = 2,248, 441 and 414 for HiFi Cas9; and *n* = 1,398 (one base), 278 (two base) and 245 (three base) for Cas9_R63A/Q768A. **d**, Activities of variants at target sequences with single-base mismatches as a function of the type of mismatch. The number of analyzed target sequences (*n*) is *n* = 214 (wobble), 237 (nonwobble) and 923 (transversion) for SpCas9; *n* = 223, 246 and 982 for Sniper1; *n* = 169, 159 and 695 for Sniper2L; *n* = 223, 236 and 934 for HiFi Cas9; and *n* = 127 (wobble), 144 (nonwobble) and 604 (transversion) for Cas9_R63A/Q768A.

is the first and only variant to gain specificity without sacrificing its general activity (Fig. 2g).

Evaluation of SpCas9 variants delivered as RNPs

SpCas9 and sgRNAs are frequently delivered in a preassembled RNP format during ex vivo genome editing therapy for human patients[14–16]. Given that delivery methods affect the on- and off-target activities of SpCas9 (ref. [17]), we compared the activities of SpCas9, Sniper1 and Sniper2L when delivered as RNPs. When individually tested at six different target sequences, we found that Sniper2L showed an overall higher on-target activity and lower off-target activity than SpCas9 (Fig. 3a and Extended Data Fig. 6), suggesting the potential advantages of Sniper2L delivered in an RNP format. We next attempted to measure the activities of high-fidelity variants, including Sniper2L, that had been delivered in RNP format into cells in a high-throughput manner (Supplementary Dataset 1). For this purpose, we utilized gRNA swapping[18] and our library of sgRNA and target sequence pairs. For accurate high-throughput evaluations, cells that do not express SpCas9 protein must be removed. When plasmids are used as the SpCas9 delivery platform, an antibiotic selection step is used for this purpose[8,19], but when the SpCas9 delivery platform is changed from plasmid to RNP, this step is no longer available. To overcome this limitation, we delivered SpCas9 protein together with an *HPRT*-targeting sgRNA. Because *HPRT* knockout provides resistance to 6-thioguanine (6-TG), the cells in which SpCas9 delivery has not occurred can be eliminated via 6-TG selection, similar to the antibiotic selection step (Supplementary Fig. 9).

HEK293T cells were transduced with library A lentivirus at an MOI (multiplicity of infection) of 0.1. After puromycin selection to remove untransduced cells, we individually transfected SpCas9, Sniper1, Sniper2L, HiFi Cas9 (ref. [6]) and Cas9_R63A/Q768A (ref. [4]), preassembled with the *HPRT*-targeting sgRNA, into the cell library. HiFi Cas9 and Cas9_R63A/Q768A were selected for comparison because HiFi Cas9 showed low off-target effects when delivered in an RNP format[6] and because Cas9_R63A/Q768A is a very recently reported high-fidelity variant of SpCas9 (ref. [4]). Then, we removed cells in which SpCas9 was not delivered by 6-TG selection, isolated genomic DNA from the surviving cells and analyzed it using deep sequencing. We found that 6-TG selection removed roughly 65–80% of the cells and dramatically increased the frequency of cells containing indels at the *HPRT* target site (Extended Data Fig. 7), indicating that cells that do not contain SpCas9 were removed. Some of the transfected SpCas9 proteins precomplexed with an *HPRT*-targeting sgRNA were expected to swap the *HPRT*-targeting sgRNA with a gRNA expressed from the transduced library[18] and then, to cleave the corresponding target sequence in the library (Supplementary Fig. 9).

Given that such RNP-based high-throughput evaluation of SpCas9 had not been conducted previously, to verify our strategy we first determined the PAM sequences that were recognized by the high-fidelity variants. Among target sequences containing all possible 4-nt PAM sequences (NNNN), variants caused the highest indel frequencies at targets with NGG PAMs, which is in line with the results from SpCas9 variant-expressing cell lines (Supplementary Fig. 10). However, activities at target sequences containing noncanonical PAM sequences,

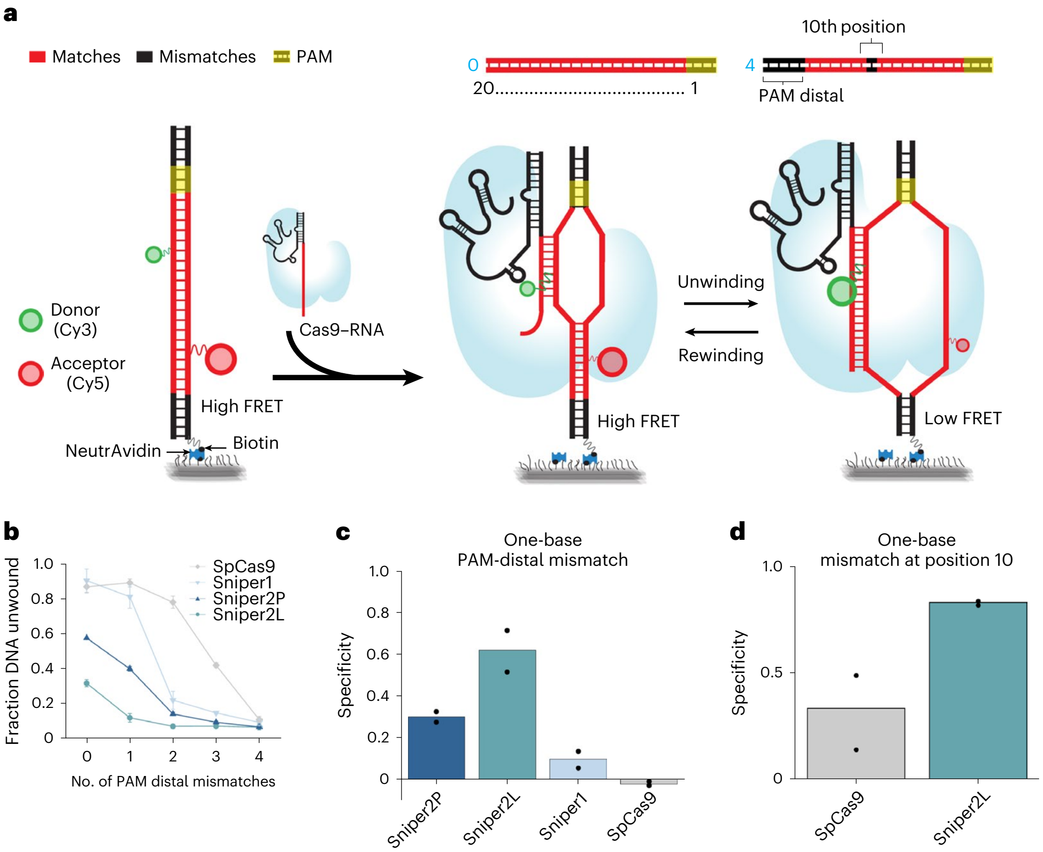

Fig. 4 | High specificity during DNA unwinding exhibited by Sniper2L, as revealed by smFRET. **a**, Schematic of the smFRET assay used to investigate SpCas9–gRNA RNP-induced unwinding of surface immobilized DNA. DNA targets (upper panel) are either a complete match to gRNAs (red) or contain mismatches (black) relative to the gRNA in the PAM-distal region or at position 10. Unwinding increases the distance between the FRET donor and acceptor, resulting in low FRET after >10 bp of DNA is unwound (FRET efficiency (E) of 0.2 to E of 0.6). **b**, f_{unwound} (equal to the relative fraction of molecules with E of 0.2 to E of 0.6) versus the number of PAM-distal mismatches n_{PD} for different SpCas9 variants. Error bars represent s.e. $n = 3$ (or more) technical replicates. **c**, Unwinding specificity for different SpCas9 variants calculated using a single PAM-distal mismatch. Bars show average specificity across experiments. Dots show specificity from each replicate. **d**, Unwinding specificity for different SpCas9 variants calculated using a mismatch at position 10. Bars show average specificity across experiments. Dots show specificity from each replicate.

such as NGA or NAG, were barely higher than 5% at most. These results suggest that the shorter time of exposure to SpCas9 (delivered in an RNP format)[17] could affect the efficiencies of the high-fidelity variants, such that they preferentially cleaved targets containing the most active PAM sequences.

We next assessed nuclease activities at 30 perfectly matched target sequences in library A and found that the activities of the high-fidelity variants were similar except that Cas9_R63A/Q768A showed a tendency toward relatively lower activities, which is in line with the previous report[4], although this difference was not statistically significant (Fig. 3b).

We also measured indel frequencies at mismatched target sequences and found that Sniper2L was highly inactive at the mismatched targets as compared with the other variants (Fig. 3c). Wobble single-base mismatches were more tolerated as compared with transversion mismatches for all variants (Fig. 3d). When we evaluated indel frequencies as a function of the mismatch position, Sniper2L hardly induced cleavage at target sequences with single-base or two- or three-base mismatches in PAM-proximal or -distal regions, a finding that is consistent with our results using lentivirus (Supplementary Figs. 11–13). Taken together, our results indicate that Sniper2L exhibits high on-target activities along with relatively low off-target activities compared with previously reported high-fidelity variants when delivered in either lentiviral or RNP format.

Single-molecular evaluation of SpCas9 variants

We next examined the fidelity of SpCas9 variants using a single-molecule approach[20]. Mechanistically, SpCas9 first binds DNA via recognition of the PAM and then, directionally unwinds the DNA protospacer from the PAM-proximal to the PAM-distal side while annealing the gRNA to the target strand[21] until ~17 base pairs are unwound[22]. At that time, SpCas9 undergoes a major conformational change involving the HNH nuclease domain to activate its nuclease activity[3,23,24], leading to the formation of a double-strand break. Mismatches between the gRNA and target sequence hinder unwinding, giving SpCas9 its sequence specificity[22]. High-fidelity SpCas9 variants show higher sequence specificity in unwinding[22,25], which shows very similar kinetics as the conformational changes involving the HNH domain[3].

To quantify the sequence specificity of the Sniper variants' DNA unwinding activity using single-molecule fluorescence resonance energy transfer (smFRET)[22,25], we used a panel of DNA sequences that contained zero to four consecutive PAM-distal mismatches (Fig. 4a). The number of PAM-distal mismatches, n_{PD}, required for more than a twofold decrease in the fraction of unwound DNA, f_{unwound}, was smaller for the high-fidelity variants ($n_{\text{PD}} \geq 3$ for SpCas9, $n_{\text{PD}} \geq 2$ for Sniper1 and Sniper2P, and $n_{\text{PD}} \geq 1$ for Sniper2L), making Sniper2L the most specific among them (Fig. 4b and Supplementary Fig. 14). The unwinding specificity, defined as $1 - (f_{\text{unwound}}$ for a target with a single mismatch divided by f_{unwound} for a perfectly matched target), was also the highest for

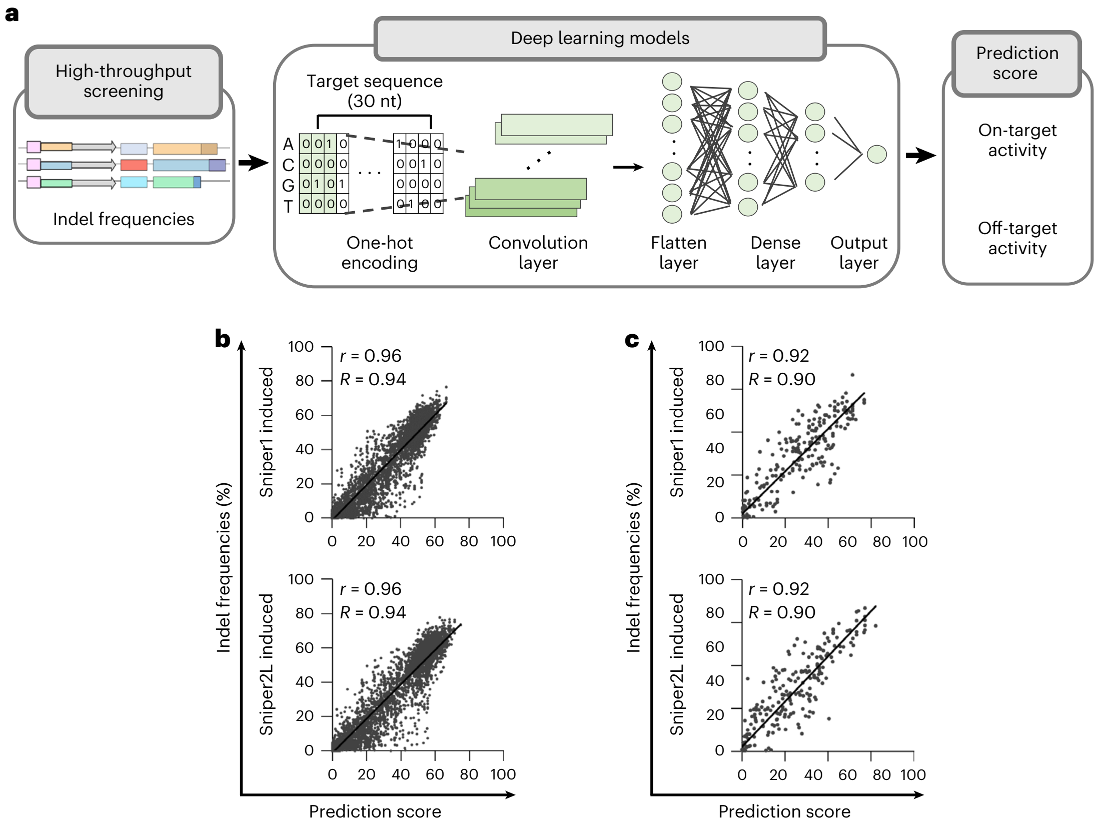

Fig. 5 | Development of deep learning-based prediction models, collectively named DeepSniper. a, A simplified schematic representation of DeepSniper development. **b**,**c**, Performance of DeepSniper in predicting the activities of Sniper1 and Sniper2L at matched (**b**) and mismatched (**c**) target sequences using target sequences that were not included in training datasets. The Pearson's correlation coefficients (*r*) and the Spearman's correlation coefficients (*R*) are presented. The number of target sequences (*n*) is *n* = 5,100 and 5,069 for Sniper1 and Sniper2L, respectively (**b**) and *n* = 295 for both Sniper1 and Sniper2L (**c**).

Sniper2L (Fig. 4c). We also tested a target sequence with or without a single mismatch at the 10th position and found that Sniper2L exhibits a superior unwinding specificity of 0.83 compared with SpCas9, with an unwinding specificity of 0.33 (Fig. 4d).

Computational models to predict Sniper2L activities

Given that the activities of Sniper2L at matched and mismatched target sequences are dependent on the target sequence, accurate prediction of Sniper2L activities would facilitate its utilization. Thus, we developed deep learning-based computational models that predict the activities of Sniper2L and Sniper1 with (G/g)N_{19} and tRNA–N_{20} sgRNAs at matched target sequences (Fig. 5a and Extended Data Fig. 8a) and with (G/g)N_{19} sgRNAs at mismatched target sequences (Extended Data Fig. 8b). We randomly divided the data obtained from libraries A, B and C in HEK293T cells lentivirally expressing Sniper2L or Sniper1 into training and test datasets (Supplementary Dataset 1). When we evaluated our models using the test datasets, we observed robust performance at both matched target sequences (Pearson's correlation coefficient *r* = 0.96, Spearman's correlation coefficient *R* = 0.94) and mismatched target sequences (*r* = 0.92, *R* = 0.90) (Fig. 5b,c). We collectively named these computational models DeepSniper, which we have provided as a web tool for wide use: http://deepcrispr.info/DeepSniper.

Discussion

In this study, we performed a directed evolution screen to generate Sniper2L, which was obtained through the addition of a further point mutation in Sniper1, a previously generated high-fidelity variant. Furthermore, compared with the previous screening approach that identified Sniper1, we used a different sgRNA and target sequence pair, which had a mismatch at a different position, and performed saturation mutagenesis at a mutational hotspot. The resulting modifications in Sniper1 allowed us to identify new variants, which were not found by using our previous approach. If we were to use a different sgRNA or a target sequence with a mismatch at a position other than the 13th, we might identify other hotspots or high-fidelity variants similar to Sniper2L and Sniper2P or identify other new variants that might be more or less specific or efficient than Sniper2L. We could also perform additional screening based on Sniper2L instead of Sniper1 or WT SpCas9. Such additional modifications in the directed evolution screen might allow us to identify other new promising variants.

Sniper2L was then characterized using two high-throughput evaluation methods, one involving lentiviral delivery and the other involving RNP delivery. Sniper2L showed higher specificity and higher general activity than Sniper1 and higher specificity and similar general activity as compared with SpCas9. Notably, this improvement shows that Sniper2L is an outlier to the previously found trade-off between general activity and specificity.

In addition, we developed a method for evaluating the activities of a large number of sgRNAs when SpCas9–sgRNA RNP complexes are delivered via electroporation. This new high-throughput method is relevant to ex vivo genome editing therapy for human patients, where the RNP delivery platform is frequently used. For successful clinical applications of CRISPR technology, the selection of an sgRNA with high activity and specificity is crucial. For this purpose, researchers often evaluate a large number of candidate sgRNAs, a process that often requires a large amount of time and money. In such situations, our high-throughput evaluation method based on SpCas9–sgRNA RNP complex delivery would facilitate sgRNA screening.

Given that 6-TG selection removed about 65–80% of the cells, the process reduced library coverage by about three- to fivefold. Thus, we filtered out sgRNA–target sequence pairs with insufficient reads (number of reads is <100) to diminish errors caused by low coverage. We think that researchers should consider this 6-TG selection-induced reduction of library coverage, which can be minimized by using highly active sgRNAs targeting *HPRT* and efficient RNP complex transfection.

In this study, we tested the activities of Cas9 variants in only one cell type, HEK293T cells. A previous report showed that the relative activities and/or specificities of SpCas9 variants were similar across different cell types, including HEK293T cells, although the absolute activities of SpCas9 variants varied depending on the cell type[6]. Thus, the relatively higher activity and specificity of Sniper2L versus that of other Cas9 variants including SpCas9 is expected to be observed in other cell types as well, and choosing Sniper2L could be an appropriate strategy for efficient and specific genome editing in a variety of cell types.

Although single-molecule unwinding analysis showed that Sniper2L has a superior discrimination against mismatched targets, its unwinding activity for a fully matched sequence was substantially lower than that of SpCas9 and Sniper1 for both of the DNA targets tested, suggesting that, for Sniper2L, the single-molecule unwinding readout does not accurately capture on-target gene editing activities. We observed DNA molecules that were stably unwound or stably rewound at a single-molecule measurement timescale of ~1 min with less than 10% showing transitions between the two states (Extended Data Fig. 9). Although SpCas9 remains stably bound to the cleavage product in vitro[21,26], inside cells, SpCas9-produced breaks are detected within minutes by the DNA repair machineries[27], suggesting that SpCas9 RNPs bound to their targets are frequently displaced. Single Sniper2L RNPs, although often bound in an inactive conformation due to conformational heterogeneity, may come on and off the on-target site multiple times during gene editing timescales of hours, yielding high gene editing activities.

The Sniper2 variants harbor amino acid substitutions in the residue E1007 of SpCas9, which is located in a region of the RuvC domain (Extended Data Fig. 10a) recently implicated to be involved in proofreading fidelity[28]. Although the role of E1007 was unclear in early crystal structures that lacked the majority of the nontarget strand[29,30], in some more recent structures that resolve the complete[31] or near-complete R loop[32–34], the E1007 side chain is positioned proximal to the 5′-phosphate of the gRNA spacer and the PAM-distal DNA duplex (Extended Data Fig. 10b). Given the implications of this region of SpCas9 to stabilize mismatches between the gRNA and PAM-distal spacer[28] to unlock nuclease domain translocations into the active catalytic state(s), we speculate that the Sniper2 E1007L/P mutations improve specificity by causing conformations less accommodating of mismatches. Future efforts to understand the precise roles of E1007 and E1007 substitutions and how they and other neighboring amino acids regulate the progression of SpCas9 into an active state may provide insight into the design of additional high-fidelity variants with distinct specificity profiles. Furthermore, how these variants impact the specificities of other CRISPR–Cas enzymes with distinct mechanistic requirements, including base editors[33,35], is an open question.

In summary, by rounds of screening following random mutagenesis, we identified Sniper2L, a new high-fidelity SpCas9 variant that exhibits an editing efficiency almost comparable with that of SpCas9, representing an outlier to the trade-off between general activity and specificity. We expect that Sniper2L will be very useful for genome editing when high efficiency and low levels of off-target effects are required.

Online content

Any methods, additional references, Nature Portfolio reporting summaries, source data, extended data, supplementary information, acknowledgements, peer review information; details of author contributions and competing interests; and statements of data and code availability are available at https://doi.org/10.1038/s41589-023-01279-5.

References

1. Slaymaker, I. M. et al. Rationally engineered Cas9 nucleases with improved specificity. *Science* **351**, 84–88 (2016).
2. Kleinstiver, B. P. et al. High-fidelity CRISPR-Cas9 nucleases with no detectable genome-wide off-target effects. *Nature* **529**, 490–495 (2016).
3. Chen, J. S. et al. Enhanced proofreading governs CRISPR-Cas9 targeting accuracy. *Nature* **550**, 407–410 (2017).
4. Bratovic, M. et al. Bridge helix arginines play a critical role in Cas9 sensitivity to mismatches. *Nat. Chem. Biol.* **16**, 587–595 (2020).
5. Casini, A. et al. A highly specific SpCas9 variant is identified by in vivo screening in yeast. *Nat. Biotechnol.* **36**, 265–271 (2018).
6. Vakulskas, C. A. et al. A high-fidelity Cas9 mutant delivered as a ribonucleoprotein complex enables efficient gene editing in human hematopoietic stem and progenitor cells. *Nat. Med.* **24**, 1216–1224 (2018).
7. Lee, J. K. et al. Directed evolution of CRISPR-Cas9 to increase its specificity. *Nat. Commun.* **9**, 3048 (2018).
8. Kim, N. et al. Prediction of the sequence-specific cleavage activity of Cas9 variants. *Nat. Biotechnol.* **38**, 1328–1336 (2020).
9. Hsu, P. D. et al. DNA targeting specificity of RNA-guided Cas9 nucleases. *Nat. Biotechnol.* **31**, 827–832 (2013).
10. Kim, H. K. et al. In vivo high-throughput profiling of CRISPR-Cpf1 activity. *Nat. Methods* **14**, 153–159 (2017).
11. Tsai, S. Q. et al. GUIDE-seq enables genome-wide profiling of off-target cleavage by CRISPR-Cas nucleases. *Nat. Biotechnol.* **33**, 187–197 (2015).
12. Zhang, D. et al. Perfectly matched 20-nucleotide guide RNA sequences enable robust genome editing using high-fidelity SpCas9 nucleases. *Genome Biol.* **18**, 191 (2017).
13. Kim, S., Bae, T., Hwang, J. & Kim, J. S. Rescue of high-specificity Cas9 variants using sgRNAs with matched 5′ nucleotides. *Genome Biol.* **18**, 218 (2017).
14. Gillmore, J. D. et al. CRISPR-Cas9 in vivo gene editing for transthyretin amyloidosis. *N. Engl. J. Med.* **385**, 493–502 (2021).
15. Frangoul, H. et al. CRISPR-Cas9 gene editing for sickle cell disease and beta-thalassemia. *N. Engl. J. Med.* **384**, 252–260 (2021).
16. Xu, L. et al. CRISPR-edited stem cells in a patient with HIV and acute lymphocytic leukemia. *N. Engl. J. Med.* **381**, 1240–1247 (2019).
17. Kim, S., Kim, D., Cho, S. W., Kim, J. & Kim, J. S. Highly efficient RNA-guided genome editing in human cells via delivery of purified Cas9 ribonucleoproteins. *Genome Res* **24**, 1012–1019 (2014).
18. Ting, P. Y. et al. Guide Swap enables genome-scale pooled CRISPR-Cas9 screening in human primary cells. *Nat. Methods* **15**, 941–946 (2018).
19. Kim, H. K. et al. SpCas9 activity prediction by DeepSpCas9, a deep learning-based model with high generalization performance. *Sci. Adv.* **5**, eaax9249 (2019).
20. Ha, T., Kaiser, C., Myong, S., Wu, B. & Xiao, J. Next generation single-molecule techniques: imaging, labeling, and manipulation in vitro and in cellulo. *Mol. Cell* **82**, 304–314 (2022).
21. Sternberg, S. H., Redding, S., Jinek, M., Greene, E. C. & Doudna, J. A. DNA interrogation by the CRISPR RNA-guided endonuclease Cas9. *Nature* **507**, 62–67 (2014).
22. Singh, D. et al. Mechanisms of improved specificity of engineered Cas9s revealed by single-molecule FRET analysis. *Nat. Struct. Mol. Biol.* **25**, 347–354 (2018).
23. Sternberg, S. H., LaFrance, B., Kaplan, M. & Doudna, J. A. Conformational control of DNA target cleavage by CRISPR-Cas9. *Nature* **527**, 110–113 (2015).

24. Yang, M. et al. The conformational dynamics of Cas9 governing DNA cleavage are revealed by single-molecule FRET. *Cell Rep.* **22**, 372–382 (2018).
25. Okafor, I. C. et al. Single molecule analysis of effects of non-canonical guide RNAs and specificity-enhancing mutations on Cas9-induced DNA unwinding. *Nucleic Acids Res.* **47**, 11880–11888 (2019).
26. Singh, D., Sternberg, S. H., Fei, J., Doudna, J. A. & Ha, T. Real-time observation of DNA recognition and rejection by the RNA-guided endonuclease Cas9. *Nat. Commun.* **7**, 12778 (2016).
27. Liu, Y. et al. Very fast CRISPR on demand. *Science* **368**, 1265–1269 (2020).
28. Bravo, J. P. K. et al. Structural basis for mismatch surveillance by CRISPR-Cas9. *Nature* **603**, 343–347 (2022).
29. Nishimasu, H. et al. Crystal structure of Cas9 in complex with guide RNA and target DNA. *Cell* **156**, 935–949 (2014).
30. Anders, C., Niewoehner, O., Duerst, A. & Jinek, M. Structural basis of PAM-dependent target DNA recognition by the Cas9 endonuclease. *Nature* **513**, 569–573 (2014).
31. Huai, C. et al. Structural insights into DNA cleavage activation of CRISPR-Cas9 system. *Nat. Commun.* **8**, 1375 (2017).
32. Jiang, F. et al. Structures of a CRISPR-Cas9 R-loop complex primed for DNA cleavage. *Science* **351**, 867–871 (2016).
33. Lapinaite, A. et al. DNA capture by a CRISPR-Cas9-guided adenine base editor. *Science* **369**, 566–571 (2020).
34. Kulcsar, P. I. et al. Blackjack mutations improve the on-target activities of increased fidelity variants of SpCas9 with 5′G-extended sgRNAs. *Nat. Commun.* **11**, 1223 (2020).
35. Porto, E. M., Komor, A. C., Slaymaker, I. M. & Yeo, G. W. Base editing: advances and therapeutic opportunities. *Nat. Rev. Drug Discov.* **19**, 839–859 2020).

Methods

Plasmid construction

Each type of plasmid used in the Sniper screen contains replication origins and resistance markers that are compatible with each other. The p11a plasmid, which contains the *ccdB* gene, was double digested with SphI and XhoI enzymes (Enzynomics) and ligated to oligos (Cosmogenetech) containing the EMX1(1.6) target sequence (gcgccacTggttgatgtgat) with T4 DNA ligase (Enzynomics). The pSC101 (sgRNA-expressing vector) and the Sniper1 library plasmid have been described previously[7]. The EMX(1.6) sgRNA sequence with a mismatch (gcgccacTggttgatgtgat; the mismatched nucleotide at position 13 is capitalized) was cloned into the pSC101 vector after BsaI digestion.

For generating plasmids that express Cas9 variants, the lentiCas9–Blast plasmid (52962; Addgene) was digested with XbaI and BamHI–HF restriction enzymes (NEB) and treated with 1 µl of calf intestinal alkaline phosphatase (NEB) for 30 min at 37 °C. The digested vector was gel purified using a MEGAquick-spin Total Fragment DNA Purification Kit (iNtRON Biotechnology) according to the manufacturer's protocol. Mutation sites were introduced into variants by amplifying the lentiCas9–Blast plasmid using primers containing the mutation (Supplementary Table 2) with Phusion High-Fidelity DNA Polymerase (NEB). The mutation sites were chosen according to suggestions from GenScript for inducing high variant expression levels[36,37]. The amplicons were gel purified (iNtRON Biotechnology) and assembled with digested lentiCas9–Blast plasmids using NEBuilder HiFi DNA Assembly Master Mix (NEB) for 1 h at 50 °C. The plasmids encoding the Sniper variants have been deposited at Addgene for distribution (138559, 193856 and 193857; Addgene).

Sniper1 mutant library construction

Sniper1 mutant libraries were constructed using three independent protocols for mutagenesis from XL1-red competent cells (Agilent), Genemorph II (Agilent) and Diversify polymerase chain reaction (PCR) random mutagenesis (Clontech) kits. All reaction conditions have been described previously[7]. The assembled libraries were transformed into Endura electrocompetent cells (Lucigen) and incubated on LB plates containing chloramphenicol (12.5 µg ml^{-1}) at 37 °C overnight. A total of 3×10^6 colonies were obtained for each library, resulting in an overall library complexity of 10^7. Pooled library plasmids were purified using a midi prep kit (NucleoBond Xtra Midi EF; Macherey-Nagel).

Positive and negative screening for directed evolution of Sniper1

BW25141–EMX1(1.6) was cotransformed with p11a (*ccdB* + target sequence) and pSC101 (sgRNA expression) plasmids (from which sgRNA expression can be induced by the addition of anhydrotetracycline (ATC)). The transformed BW25141–EMX1 cells were plated on LB plates containing ampicillin (50 µg ml^{-1}) and kanamycin (25 µg ml^{-1}) and then, incubated overnight at 32 °C. Electrocompetent cells were produced from transformants cultured in liquid super optimal broth medium containing 0.1% glucose, ampicillin and kanamycin until the optical density at 600 nm reached 0.4. Each Sniper library underwent four rounds of screening; 100 ng of plasmids from each library were transformed into 50 µl of electrocompetent BW25141–EMX1(1.6) cells using a Gene Pulser (Gene Pulser II; Bio-Rad) following the manufacturer's instructions. In the first round of screening, the transformed cells were initially incubated without ATC and then, plated on LB plates containing chloramphenicol and kanamycin (nonselective conditions) and LB plates containing chloramphenicol, kanamycin and 1.5 mg ml^{-1} arabinose (Sigma-Aldrich; selective conditions) without ATC followed by overnight culture at 32 °C. In the second to fourth rounds of screening, the transformed cells were incubated with 10 ng ml^{-1} ATC during recovery and then, plated on nonselective and selective LB plates in the absence of ATC. Sniper screening conditions have been described previously[7]. After four rounds of screening, 50 colonies were obtained from selective plates and then, incubated in chloramphenicol-containing LB medium at 42 °C. Each plasmid was Sanger sequenced.

Site saturation mutagenesis at a hotspot in Sniper1

For site saturation mutagenesis of the 1,007th codon in the Sniper1 sequence, the pBLC–Sniper1 plasmid was amplified using primers containing NNK (K = G or T) at the appropriate position (forward primer: agtaccccaagctggagagcnnkttcgtgtacggcgactacaagg; reverse primer: tcttgatcagggcggtgcc). PCR products were digested with DpnI (Enzynomics), treated with T4 polynucleotide kinase (Enzynomics) and ligated with T4 ligase (Enzynomics). The resulting product was transformed in DH5alpha cells. After Sanger sequencing of plasmids from 100 randomly selected colonies, variants containing 20 different amino acids at the 1,007th position were identified.

Oligonucleotide libraries

Three oligonucleotide pools, libraries A, B and C, were described in our previous study[8]. Library A was utilized for evaluating PAM sequences and activities at mismatched target sequences. Using library B, indel frequencies induced by variants were measured at a large number of target sequences with (G/g)N_{19} sgRNAs. Library C contained target sequences that were identical with those in library B but used a different sgRNA expression system that resulted in perfectly matched tRNA–N_{20} sgRNAs. All three oligonucleotide libraries were used for examining Sniper1 variants based on lentiviral delivery, whereas library A was applied for comparing high-fidelity variants using the RNP delivery method.

Cell culture and transfection

HEK293T cells were maintained in DMEM supplemented with 100 U ml^{-1} penicillin, 100 mg ml^{-1} streptomycin and 10% FBS. Cells were transfected using lipofectamine 2000 (Invitrogen) at a weight ratio of 1:1 (Sniper1 variant plasmid:sgRNA expression plasmid) in 48-well plates. Genomic DNA was isolated with a DNeasy Blood & Tissue Kit (Qiagen) 72 h after transfection.

Production of lentivirus

Lentivirus was produced using a method identical to that utilized in our previous study[8]. In brief, the day before transfection, HEK293T cells were seeded; the following day, the cells were treated with chloroquine diphosphate for up to 5 h and transfected with lentiviral vector and packaging plasmids. The next day, the lentivirus-containing medium was removed, and fresh DMEM was added to the transfected HEK293T cells. The supernatant with viral particles was harvested 48 h after transfection; remaining library plasmids were degraded by treatment with Benzonase (Enzynomics)[38,39].

Generation of Sniper1 variant-expressing cell lines and transduction of lentiviral libraries

For measuring lentiviral titers, HEK293T cells were transduced with sequentially diluted aliquots of lentivirus-containing supernatant along with 10 µg ml^{-1} polybrene and incubated overnight. The next day, both transduced and untransduced cells were treated with 20 µg ml^{-1} blasticidin S (InvivoGen), and the number of surviving cells in the transduced population was counted when the untransduced cells were no longer viable[38]. Cell lines expressing Sniper1 variants were continuously maintained in the presence of 20 µg ml^{-1} blasticidin S (InvivoGen).

Lentiviral libraries were transduced into Sniper1 variant-expressing cells using a protocol identical with that previously described[8]. In brief, 2.5×10^7 Sniper1 variant-expressing cells were seeded in each 15-cm dish; two dishes (with a total of 5×10^7 cells) were used for libraries A and C, and four dishes (with a total of 1.0×10^8 cells) were used for library B. Lentiviral plasmid libraries were transduced at an MOI of 0.4 along with 10 µg ml^{-1} polybrene. After 4 days (libraries A, B and C) and 7 days (library A) of transduction, cells were harvested.

For generating variant-expressing cell lines, we generated a mother batch of HEK293T cells, aliquoted it and stored the aliquots in a liquid nitrogen tank. To directly compare the variants, we used these frozen, aliquoted HEK293T cells for our previously published[8] and current studies within a limited number of passages. For all Cas9 variant experiments, we thawed an aliquot of mother cells, passaged the cells twice and transduced them with lentivirus expressing a Cas9 variant. At four passages after the transduction, we aliquoted the cells and stored the aliquots in a liquid nitrogen tank. After thawing an aliquot of the Cas9-expressing cells, we passaged the cells twice and treated them with a lentiviral library of sgRNA-encoding and target sequence pairs (for example, library A, B or C).

Western blotting

Levels of Sniper1, Sniper2L and Sniper2P proteins were determined with western blotting using purified anti-CRISPR–Cas9 (diluted 1:1,000, 844301; Biolegend) and anti-β-actin (diluted 1:1,000, sc-47778; Santa Cruz Biotechnology) primary antibodies. Horseradish peroxidase-conjugated goat anti-mouse immunoglobulin G antibody (diluted 1:5,000, sc-516102; Santa Cruz Biotechnology) was used for signal detection.

Deep sequencing and analysis

To examine the activities of the Sniper1 variants, samples were prepared and analyzed as previously described[8]. The following formula was used to remove background indel frequencies:

$$\text{Indel frequencies}\,(\%) = \frac{\text{Indel read counts}-(\text{Total read counts}\times\text{background indel frequency})/100}{\text{Total read counts}-(\text{Total read counts}\times\text{background indel frequences})/100}\times 100.$$

To minimize the errors generated by array synthesis, PCR amplification or deep sequencing, we excluded target sequences with fewer than 100 total read counts or that exhibited background indel frequencies greater than 8% from the analysis.

RNP-based delivery of SpCas9 variants into a cell library

Lentiviral plasmid library A was transduced into HEK293T cells at an MOI of 0.1 to generate a cell library. The cell library was continuously maintained in the presence of 2 μg ml^{-1} puromycin (Invitrogen). The *HPRT*-targeting sgRNA templates were generated by annealing two complementary oligonucleotides, which were then incubated with T7 RNA polymerase in reaction buffer (40 mM Tris HCl, 6 mM $MgCl_2$, 10 mM DTT, 10 mM NaCl, 2 mM spermidine, 3.3 mM NTPs and 1 U μl^{-1} RNase inhibitor at pH 7.9) for 8 h at 37 °C. Transcribed sgRNAs were preincubated with DNase I to remove template DNA and purified using a PCR purification kit (Macrogen). A total of 3×10^7 cells (6×10^6 cells per dish × 5 dishes) were transfected with protein variants (WT SpCas9, Sniper1, Sniper2L, HiFi Cas9 and Cas9_R63A/Q768A; 40 μg) premixed with in vitro-transcribed *HPRT*-targeting sgRNA (40 μg) and Alt-R Cas9 electroporation enhancer (4 μM; Integrated DNA Technologies) using a Neon transfection system (ThermoFisher) with the following settings: 1,150 V, 20 ms and two pulses per 2×10^6 cells using a 100-μl tip. On day 3 after transfection, a portion of the cell culture was harvested for analysis of indels at the *HRPT* site. Beginning on day 7 after transfection, cells were maintained in DMEM supplemented with 10% FBS and 30 μM 6-TG (Sigma). The cells were harvested 14 days after the 6-TG selection began. Genomic DNA was isolated with a Blood & Cell Culture DNA Maxi Kit (Qiagen).

Preparation of DNA targets for single-molecule experiments

Integrated DNA Technologies supplied all DNA oligonucleotides. For introducing Cy3 and Cy5 labels on the target strand at the 6th position and the nontarget strand at the 16th position, respectively (indicated in Fig. 4a and Supplementary Table 3), the oligonucleotides were synthesized with amine-containing modified thymines at the appropriate locations. A C6 linker (amino-dT) was used to label the DNA strands with Cy3 or Cy5 *N*-hydroxysuccinimido. For preparing the DNA, the nontarget strand, target strand, and a 22-nt biotinylated adapter strand were first mixed in a solution containing 10 mM Tris HCl, pH 8 and 50 mM NaCl. The mixture was transferred to a heat block preheated to 90 °C. After 2 min of heating, the mixture was cooled to room temperature over a few hours. The sequences of the target and nontarget strands (with the same label positions) were changed to create DNA targets with mismatches. The full sequences of all DNA targets used in the smFRET assay are shown in Supplementary Table 3.

Preparation of gRNAs and SpCas9–gRNA RNPs for single-molecule experiments

crRNAs and tracrRNAs were synthesized by Integrated DNA Technologies. All gRNAs were prepared by mixing CRISPR RNA (crRNA; 10 μM) and trans-activating crRNA (tracrRNA; 12 μM) in a 1:1.2 ratio in a solution containing 10 mM Tris HCl, pH 8 and 50 mM NaCl. This mixture was then placed in a heating block preheated to 90 °C for 2 min, after which it was allowed to cool to room temperature over a few hours for efficient hybridization between the crRNA and tracrRNA. SpCas9–gRNA RNPs were prepared by mixing the gRNA (1 μM) and SpCas9 (2 μM) at a ratio of 1:2 in SpCas9–gRNA activity buffer, which consisted of 20 mM Tris HCl, pH 8, 100 mM KCl, 5 mM $MgCl_2$ and 5% (vol/vol) glycerol (final concentration: 500 nM). The full sequences of all of the gRNAs used in this study are available in Supplementary Table 3.

Single-molecule fluorescence imaging and data analysis

Flow chamber surfaces coated with polyethylene glycol were used for immobilization of DNA targets. The flow chambers were purchased from the Johns Hopkins University Microscope Supplies Core. The neutrAvidin–biotin interaction was used for immobilizing the biotinylated DNA target molecules on the polyethylene glycol-passivated flow chamber surfaces in Cas9–RNA activity and imaging buffer without glucose oxidase and catalase (20 mM Tris HCl, 100 mM KCl, 5 mM $MgCl_2$, 5% (vol/vol) glycerol, 0.2 mg ml^{-1} BSA, 0.8% dextrose and saturated Trolox (>5 mM))[20]. SpCas9–gRNA RNPs in Cas9–RNA activity and imaging buffer with catalase and glucose oxidase (20 mM Tris HCl, 100 mM KCl, 5 mM $MgCl_2$, 5% (vol/vol) glycerol, 0.2 mg ml^{-1} BSA, 1 mg ml^{-1} glucose oxidase, 0.04 mg ml^{-1} catalase, 0.8% dextrose and saturated Trolox (>5 mM)) were added to the flow chamber at concentrations that were much higher (for example, 100 nM) than the dissociation constant of the SpCas9–gRNA–DNA complex for SpCas9–gRNA targeting of DNA and SpCas9–gRNA RNP-induced DNA unwinding. All of the imaging experiments were done at room temperature, and the time resolution was either 100 or 35 ms per frame. The total fluorescence from each of the immobilized DNA target molecules was optically split into two separate donor and acceptor optical paths. The emissions belonging to these two parts were projected onto two halves of a cryocooled (<−70 °C) electron-multiplying charge-coupled device camera (Andor) and were then stored as a video recording by the camera. The video recording containing fluorescent spots was then analyzed using custom scripts to extract background-corrected donor fluorescence (I_D) and acceptor fluorescence (I_A). The fluorescence resonance energy transfer (FRET) efficiency (E) of each detected spot was approximated as $E = I_A/(I_D + I_A)$. In the analysis of the DNA unwinding experiments, the DNA molecules with missing or inactive acceptor labels were avoided by only including the fluorescent spots in the acceptor channel. The data acquisition software and analysis scripts can be downloaded from GitHub (https://github.com/Ha-SingleMoleculeLab). A detailed explanation of smFRET data acquisition and analysis has previously been described[40].

E histograms and analysis of SpCas9–gRNA RNP-induced DNA unwinding and rewinding

For every single molecule, the first five data points of its *E* time traces were used as data points to construct *E* histograms. More than 2,000 molecules contributed to each E histogram. The donor-only peak ($E = 0$), low-FRET ($0.2 < E < 0.6$, 0.65 or 0.70) population and high-FRET ($E > 0.6$, 0.65 or 0.7) population are three characteristic populations observed in these E histograms. Based on these low- and high-FRET populations, SpCas9–gRNA RNP-induced DNA unwinding was modeled as a two-state system, as shown below. The unwound fraction (f_{unwound}) was calculated as a fraction of the low-FRET population in the E histograms from the DNA unwinding experiments.

Deep learning models

Our data were randomly divided into training and test datasets, and fivefold crossvalidation was applied. For on-target prediction models, 32,109 and 31,810 target sequences were used for Sniper1 and Sniper2L, respectively (Supplementary Dataset 1); 2,656 and 2,654 target sequences were utilized for training the off-target prediction models for Sniper1 and Sniper2L, respectively (Supplementary Dataset 1). The numbers of target sequences that were used for evaluating the models are indicated in Fig. 5b,c.

To develop on-target activity prediction models, the 30-nt target sequences were one-hot encoded to generate numerical inputs of the convolution layers, and zero padding was utilized for retaining the number of target sequences. The features of the input sequences were extracted using the first convolution layer with 256 filters 5 nt in length for both Sniper1 and Sniper2L followed by average pooling layers, which were then flattened. Two fully connected layers with 1,500 nodes and one fully connected layer with 100 nodes were used for both Sniper1 and Sniper2L. To consider whether $(G/g)N_{19}$ or tRNA–N_{20} sgRNA expression systems should be adopted, they were indicated as a binary value. The features of a binary value were converted into a 100-dimensional vector and multiplied with the output of the third fully connected layer to integrate features of target sequence compositions and sgRNA expression systems. The final prediction scores were generated by performing a linear transformation of the output of the multiplication.

To develop off-target activity prediction models, the 20-nt sgRNA sequences and mismatched targets were one-hot encoded to make numerical inputs of the convolution layers, and zero padding was used for sustaining the number of target sequences. The features of the input sequences were extracted using the first convolution layer with 128 filters 3 and 5 nt in length for Sniper1 and Sniper2L, respectively, followed by average pooling layers, which were then flattened. As another input, the identities of mismatched nucleotides were given as numerical values, and those were concatenated with the output of the flatten layer. Three fully connected layers with 1,500 nodes and one fully connected layer with 100 nodes were utilized for both Sniper1 and Sniper2L, and information about the sgRNA expression systems was not provided. The final prediction scores were generated by performing a linear transformation of the output of the multiplication.

Dropout layers with a rate of 0.3 were applied to avoid overfitting. The rectified linear unit was adopted for the convolution and dense layers. As the loss function, a mean absolute error was utilized, and an Adam optimizer with a learning rate of 10^{-4} was applied. TensorFlow v.2.5 was used for developing our models[41].

Statistical significance

Results from the Kruskal–Wallis test and the Mann–Whitney U test calculated by SPSS Statistics (v.25; IBM) are shown. We used GraphPad Prism 5 to draw graphs.

Reporting summary

Further information on research design is available in the Nature Portfolio Reporting Summary linked to this article.

Data availability

We have submitted the deep sequencing data from this study to the NCBI Sequence Read Archive under accession number PRJNA817000. We have provided the datasets used in this study as Supplementary Dataset 1. We used PDB IDs 5Y36 (ref. [31]) and 6VPC (ref. [28]) for structural analyses shown in Extended Data Fig. 10. Source data are provided with this paper.

Code availability

We have made the source code for DeepSniper and analyzing FRET data available on GitHub at https://github.com/NahyeKim/DeepSniper and http://github.com/Ha-SingleMoleculeLab.

References

36. Koblan, L. W. et al. Improving cytidine and adenine base editors by expression optimization and ancestral reconstruction. *Nat. Biotechnol.* **36**, 843–846 (2018).
37. Zafra, M. P. et al. Optimized base editors enable efficient editing in cells, organoids and mice. *Nat. Biotechnol.* **36**, 888–893 (2018).
38. Sastry, L., Xu, Y., Cooper, R., Pollok, K. & Cornetta, K. Evaluation of plasmid DNA removal from lentiviral vectors by benzonase treatment. *Hum. Gene Ther.* **15**, 221–226 (2004).
39. Sack, L. M., Davoli, T., Xu, Q., Li, M. Z. & Elledge, S. J. Sources of error in mammalian genetic screens. *G3 (Bethesda)* **6**, 2781–2790 (2016).
40. Joo, C. & Ha, T. Single-molecule FRET with total internal reflection microscopy. *Cold Spring Harb. Protoc.* https://doi.org/10.1101/pdb.top072058 (2012).
41. Abadi, M. et al. TensorFlow: a system for large-scale machine learning. Preprint at *arXiv* https://doi.org/10.48550/arXiv.1605.08695 (2016).

Acknowledgements

We thank Y. Kim and S. Park for assisting with the experiments and M. Song for providing technical advice. This work was supported in part by the 'Alchemist Project' funded by the Ministry of Trade, Industry and Energy (20012443 to J.K.L.); the National Research Foundation of Korea funded by the Korean government (Ministry of Science and ICT (MSIT); 2022R1A3B1078084 to H.H.K., 2018R1A5A2025079 to H.H.K. and 2022R1C1C2004229 to N.K.); the Yonsei Signature Research Cluster Program of 2021-22-0014 (to H.H.K.); the Brain Korea 21 FOUR Project for Medical Science (Yonsei University College of Medicine); the Korean Health Technology R&D Project, Ministry of Health and Welfare, Republic of Korea (HI21C1314 to H.H.K.); and the US National Institutes of Health (R35 GM122569). T.H. is an investigator with the Howard Hughes Medical Institute (HHMI). This article is subject to HHMI's Open Access to Publications policy. HHMI laboratory heads have previously granted a nonexclusive CC BY 4.0 license to the public and a sublicensable license to HHMI in their research articles. Pursuant to those licenses, the author-accepted manuscript of this article can be made freely available under a CC BY 4.0 license immediately upon publication. B.P.K. acknowledges support from a Mass General Hospital Howard M. Goodman Fellowship.

Author contributions

Y.K., N.K., J.L., S.-M.B. and K.C. performed the experiments. Y.K., N.K., H.H.K., T.H. and J.K.L. designed the study and wrote the manuscript. S.C. and S.M. developed computational models. Y.-h.K. and J.-S.K. provided valuable advice during the project. I.O., J.C. and V.H. performed single-molecule measurements and analysis under supervision by T.H. B.P.K. contributed to structural modeling of SpCas9 mutations.

Competing interests

A patent application has been filed based on this work: Toolgen filed 10-2019-0049115 (Status: Published Case, Inventor: J.L. and J.K.L.) covering Sniper2L. B.P.K. is an inventor on patents and/or patent applications filed by Mass General Brigham that describe genome engineering technologies. B.P.K. is a consultant for EcoR1 capital and is a scientific advisor to Acrigen Biosciences, Life Edit Therapeutics and Prime Medicine. H.H.K. is a consultant for EcoR1 capital. The remaining authors declare no competing interests.

Additional information

Extended data is available for this paper at https://doi.org/10.1038/s41589-023-01279-5.

Supplementary information The online version contains supplementary material available at https://doi.org/10.1038/s41589-023-01279-5.

Correspondence and requests for materials should be addressed to Jungjoon K. Lee, Taekjip Ha or Hyongbum Henry Kim.

Peer review information *Nature Chemical Biology* thanks Sungchul Kim, Keiichiro Suzuki and the other, anonymous, reviewer(s) for their contribution to the peer review of this work.

Reprints and permissions information is available at www.nature.com/reprints.

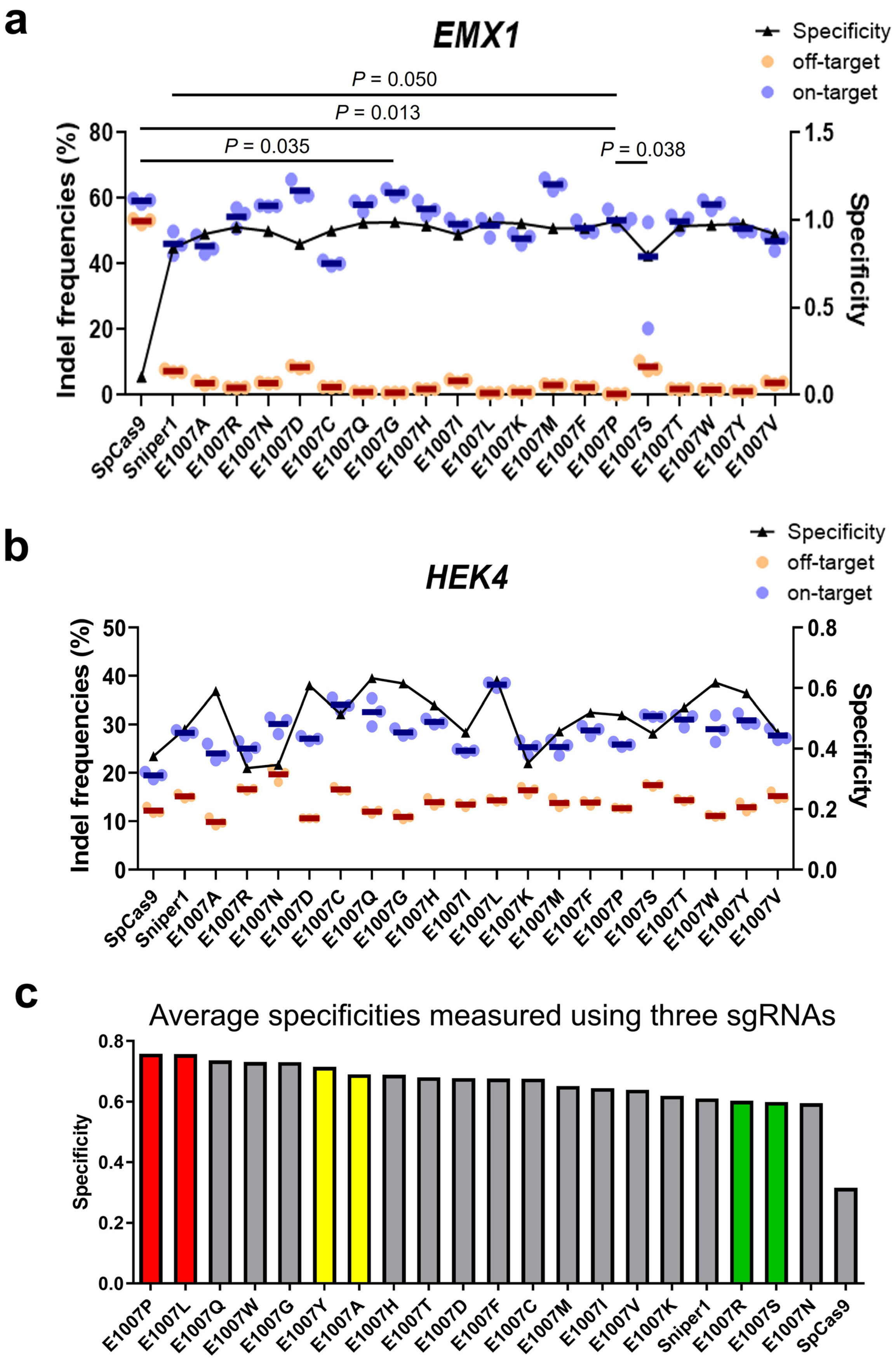

Extended Data Fig. 1 | See next page for caption.

Extended Data Fig. 1 | Indel frequencies at on- (blue) and off- (orange) target sites and specificities determined after transfection of plasmids encoding SpCas9 or Sniper-Cas9 variants into HEK293T cells. Sniper-Cas9 variants were generated by site saturation mutagenesis at the 1007th amino acid codon (originally a Glu codon); the resulting amino acids at that position are shown on the x-axis. Indel frequencies and specificities are shown on the left and right y-axes, respectively. Specificity was calculated as 1 – (indel frequencies at off-target sequences divided by those at on-target sequences). The averages of three replicates are indicated by dark blue and red horizontal lines. The name of the gene in which the target sequence is located is indicated at the top of each graph. **a, b**, The number of independent transfections *n* = 3. Statistical significances are shown (no statistical significance (P > 0.05) unless specified in the figure; Kruskal-Wallis test). As the target sequence, another sequence (not the EMX1.6 sgRNA-corresponding sequence) in the human *EMX1* gene was used (**a**). **c**, Average specificities of Sniper1, 19 Sniper1 variants with amino acid substitutions at the 1007th position, and SpCas9 determined using sgRNAs targeting three sites (*EMX1, ZSCAN2*, and *HEK4*). The two variants with the highest average specificities (that is, E1007L and E1007P) are indicated using red bars. Four randomly selected variants that were also evaluated using sgRNAs targeting eight sites (shown in Supplementary Fig. 5) are represented using either yellow or green bars.

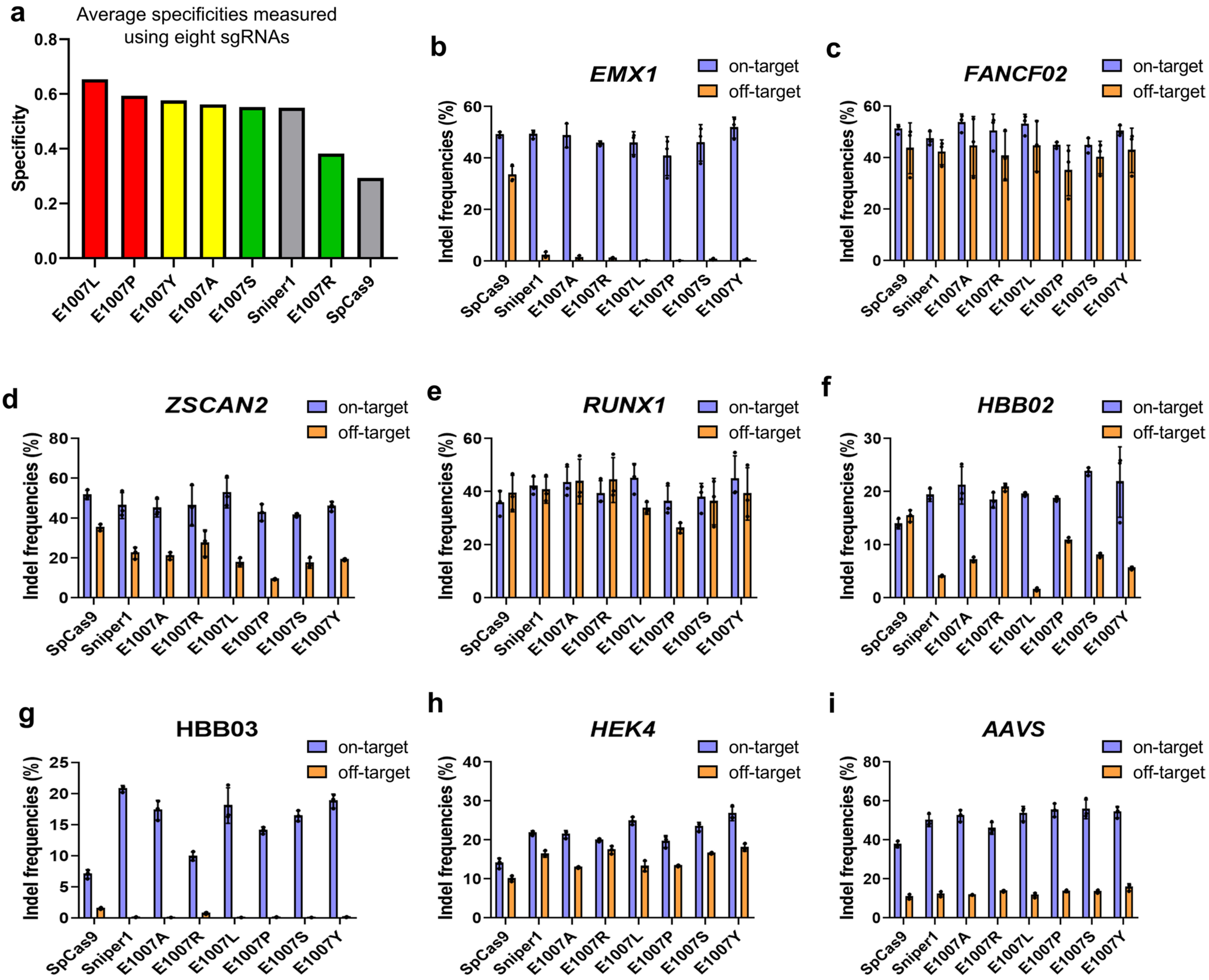

Extended Data Fig. 2 | Indel frequencies induced by plasmid-based transfection of SpCas9 and Sniper-Cas9 variants at on- (blue) and off- (orange) target sequences in HEK293T cells. a, Average specificities of Sniper1, six Sniper1 variants with amino acid substitutions at the 1007th position, and SpCas9 measured using sgRNAs targeting eight sites (*EMX1, ZSCAN2, HEK4, FANCF02, RUNX1, HBB02, HBB03*, and *AAVS*). The bars are color-coded as in Supplementary Fig. 4c: the two variants with the highest average specificities are indicated using red bars and the four randomly selected variants are represented with either yellow or green bars. **b-i**, Indel frequencies are shown on the y-axes. Summarized results for the eight target sequences are shown in Fig. 1c, d and Supplementary Fig. 5a. Error bars indicate s.e.m. The number of independent transfections $n = 3$.

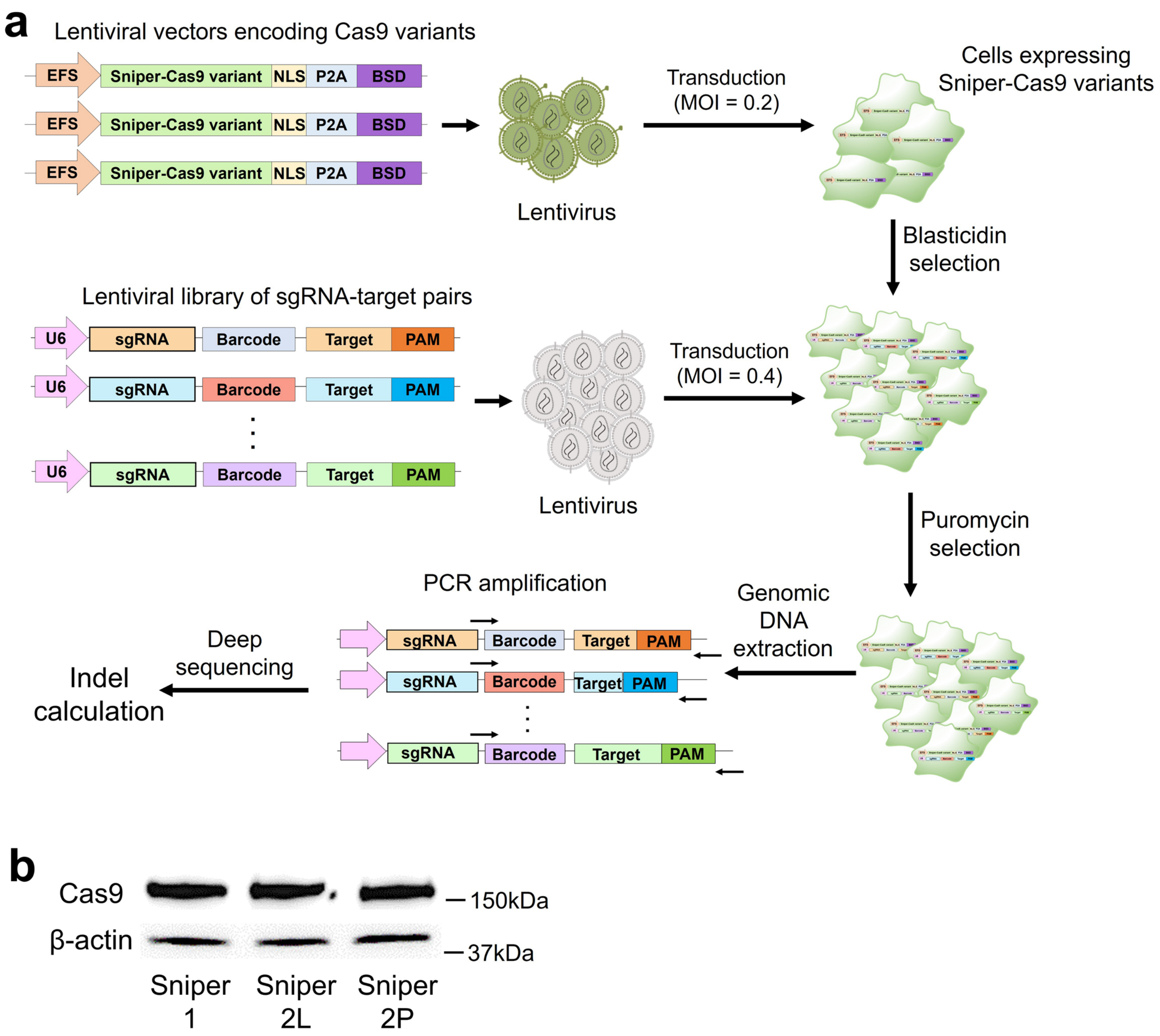

Extended Data Fig. 3 | Generation and examination of Sniper-Cas9 variant-expressing cell lines. a, Schematic representation of the generation of cell lines expressing Sniper-Cas9 variants and the subsequent evaluation of Sniper-Cas9 variants at a large number of target sequences. **b**, Western blot analysis to determine the level of expressed SpCas9 proteins in the Sniper-Cas9 variant-expressing cell lines. The result from a single western blot analysis is shown.

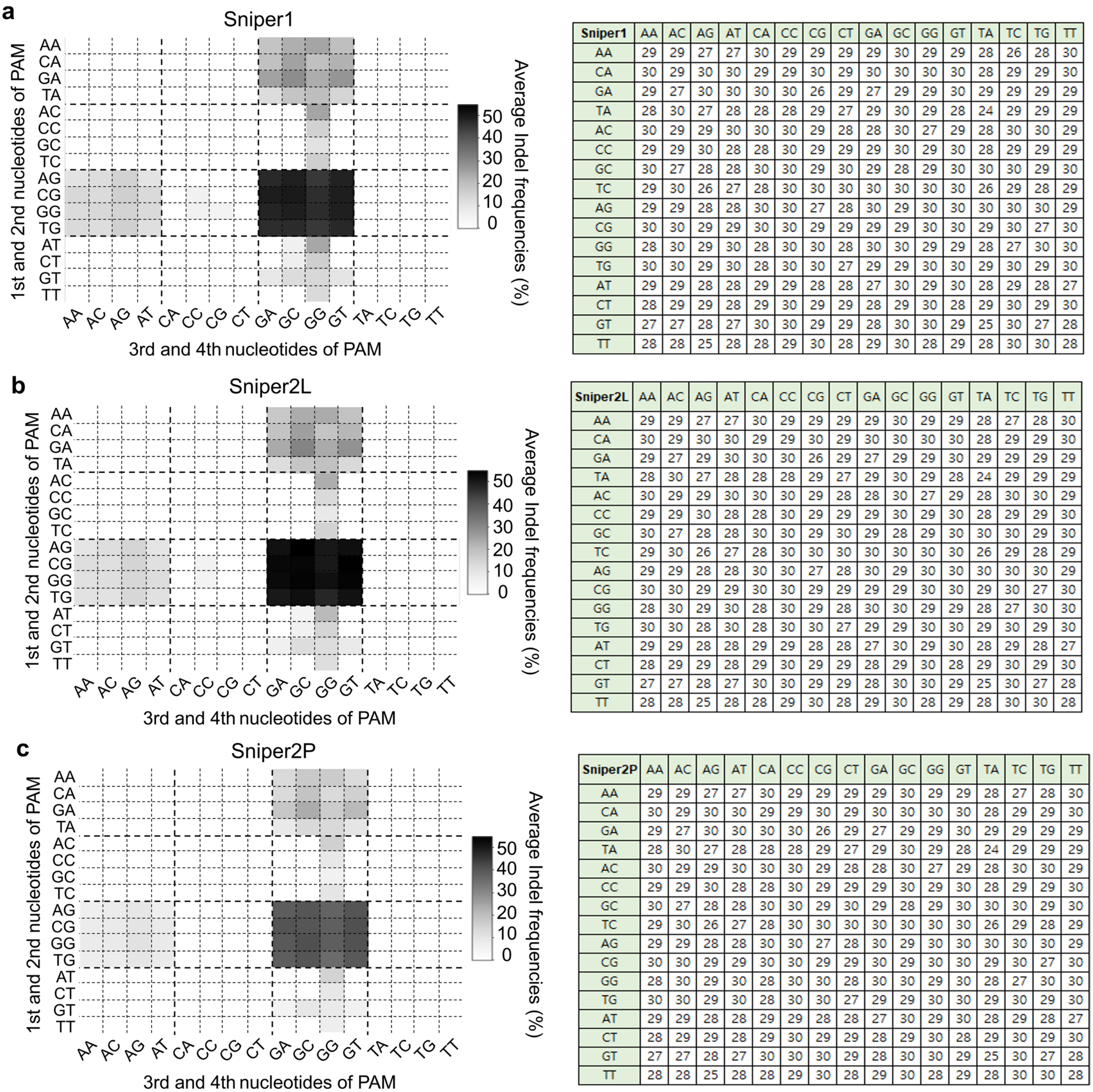

Sniper1	AA	AC	AG	AT	CA	CC	CG	CT	GA	GC	GG	GT	TA	TC	TG	TT
AA	29	29	27	27	30	29	29	29	29	30	29	29	28	26	28	30
CA	30	29	30	30	29	29	30	29	30	30	30	30	28	29	29	30
GA	29	27	30	30	30	30	26	29	27	29	29	30	29	29	29	29
TA	28	30	27	28	28	28	29	27	29	30	29	28	24	29	29	29
AC	30	29	29	30	30	30	29	28	28	30	27	29	28	30	30	29
CC	29	29	30	28	28	30	29	29	29	30	29	30	28	29	29	29
GC	30	27	28	28	30	30	29	30	29	28	29	30	30	30	29	30
TC	29	30	26	27	28	30	30	30	30	30	30	30	26	29	28	29
AG	29	29	28	28	30	30	27	28	30	29	30	30	30	30	30	29
CG	30	30	29	29	30	30	29	29	29	29	30	30	29	30	27	30
GG	28	30	29	30	28	30	30	28	30	30	29	29	28	27	30	30
TG	30	30	29	30	28	30	30	27	29	29	30	30	29	30	29	30
AT	29	29	28	28	29	29	28	28	27	30	29	30	28	29	28	27
CT	28	29	29	28	29	30	29	29	28	29	30	28	29	30	29	30
GT	27	27	28	27	30	30	29	29	28	30	30	29	25	30	27	28
TT	28	28	25	28	28	29	30	28	29	30	28	29	28	30	30	28

Sniper2L	AA	AC	AG	AT	CA	CC	CG	CT	GA	GC	GG	GT	TA	TC	TG	TT
AA	29	29	27	27	30	29	29	29	29	30	29	29	28	27	28	30
CA	30	29	30	30	29	29	30	29	30	30	30	30	28	29	29	30
GA	29	27	29	30	30	30	26	29	27	29	29	30	29	29	29	29
TA	28	30	27	28	28	28	29	27	29	30	29	28	24	29	29	29
AC	30	29	29	30	30	30	29	28	28	30	27	29	28	30	30	29
CC	29	29	30	28	28	30	29	29	29	30	29	30	28	29	29	30
GC	30	27	28	28	30	30	29	30	29	28	29	30	30	30	29	30
TC	29	30	26	27	28	30	30	30	30	30	30	30	26	29	28	29
AG	29	29	28	28	30	30	27	28	30	29	30	30	30	30	30	29
CG	30	30	29	29	30	30	29	29	29	29	30	30	29	30	27	30
GG	28	30	29	30	28	30	29	28	30	30	29	29	28	27	30	30
TG	30	30	28	30	28	30	30	27	29	29	30	30	29	30	29	30
AT	29	29	28	28	29	29	28	28	27	30	29	30	28	29	28	27
CT	28	29	29	28	29	30	29	29	28	29	30	28	29	30	29	30
GT	27	27	28	27	30	30	29	29	28	30	30	29	25	30	27	28
TT	28	28	25	28	28	29	30	28	29	30	28	29	28	30	30	28

Sniper2P	AA	AC	AG	AT	CA	CC	CG	CT	GA	GC	GG	GT	TA	TC	TG	TT
AA	29	29	27	27	30	29	29	29	29	30	29	29	28	27	28	30
CA	30	29	30	30	29	29	30	29	30	30	30	30	28	29	29	30
GA	29	27	30	30	30	30	26	29	27	29	29	30	29	29	29	29
TA	28	30	27	28	28	28	29	27	29	30	29	28	24	29	29	29
AC	30	29	29	30	30	30	29	28	28	30	27	29	28	30	30	29
CC	29	29	30	28	28	30	29	29	29	30	29	30	28	29	29	30
GC	30	27	28	28	30	30	29	30	29	28	29	30	30	30	29	30
TC	29	30	26	27	28	30	30	30	30	30	30	30	26	29	28	29
AG	29	29	28	28	30	30	27	28	30	29	30	30	30	30	30	29
CG	30	30	29	29	30	30	29	29	30	29	30	30	29	30	27	30
GG	28	30	29	30	28	30	30	28	30	30	29	30	28	27	30	30
TG	30	30	29	30	28	30	30	27	29	29	30	30	29	30	29	30
AT	29	29	28	28	29	29	28	28	27	30	29	30	28	29	28	27
CT	28	29	29	28	29	30	29	29	28	29	30	28	29	30	29	30
GT	27	27	28	27	30	30	30	29	28	30	30	29	25	30	27	28
TT	28	28	25	28	28	29	30	28	29	30	28	29	28	30	30	28

Extended Data Fig. 4 | PAM sequences recognized by Sniper1 (a), Sniper2L (b), and Sniper2P (c). Average indel frequencies four days after the transduction of library A into Sniper-Cas9 variant-expressing cells are shown; average indel frequencies lower than 5% are indicated as white boxes in the grids. The number of target sequences per each 4-nt PAM (*n*) are shown in the right tables.

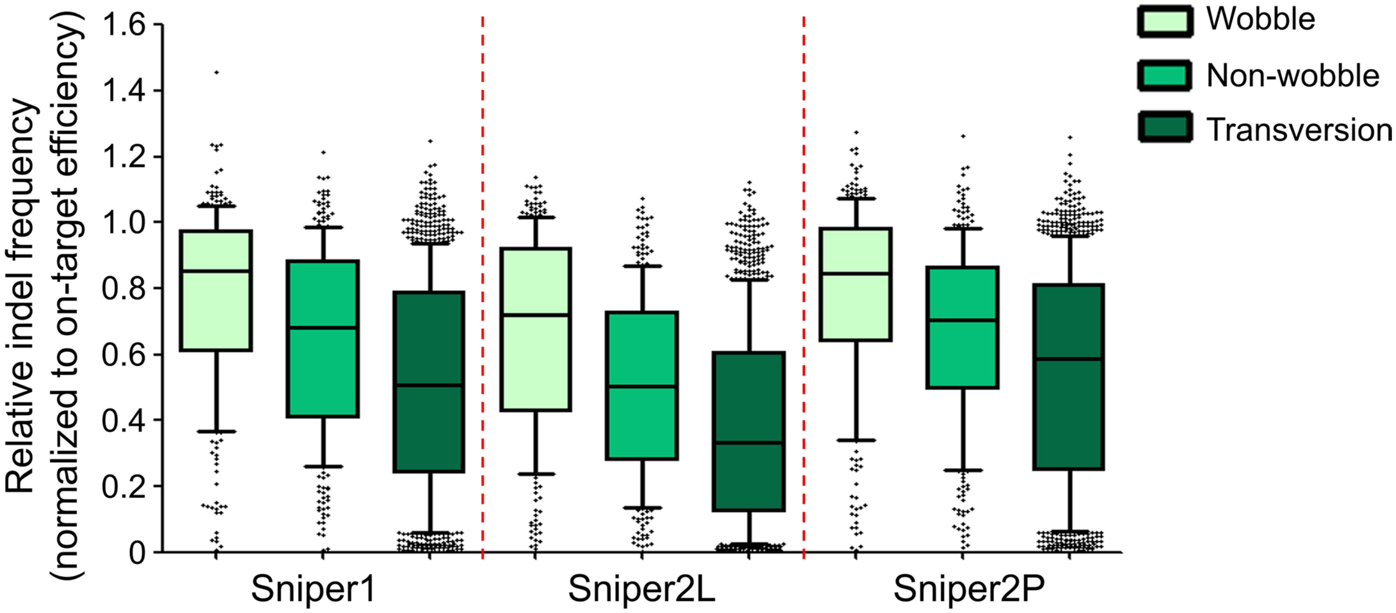

Extended Data Fig. 5 | Relative indel frequencies induced by Sniper1, Sniper2L, and Sniper2P at mismatched targets vary depending on the type of single-base mismatches. The boxes represent the 25th, 50th, and 75th percentiles; whiskers show the 10th and 90th percentiles. *n* = 275 (wobble), 304 (non-wobble), and 1,155 (transversion) mismatches for Sniper1 and Sniper2P and 275, 304, and 1,153 for Sniper2L.

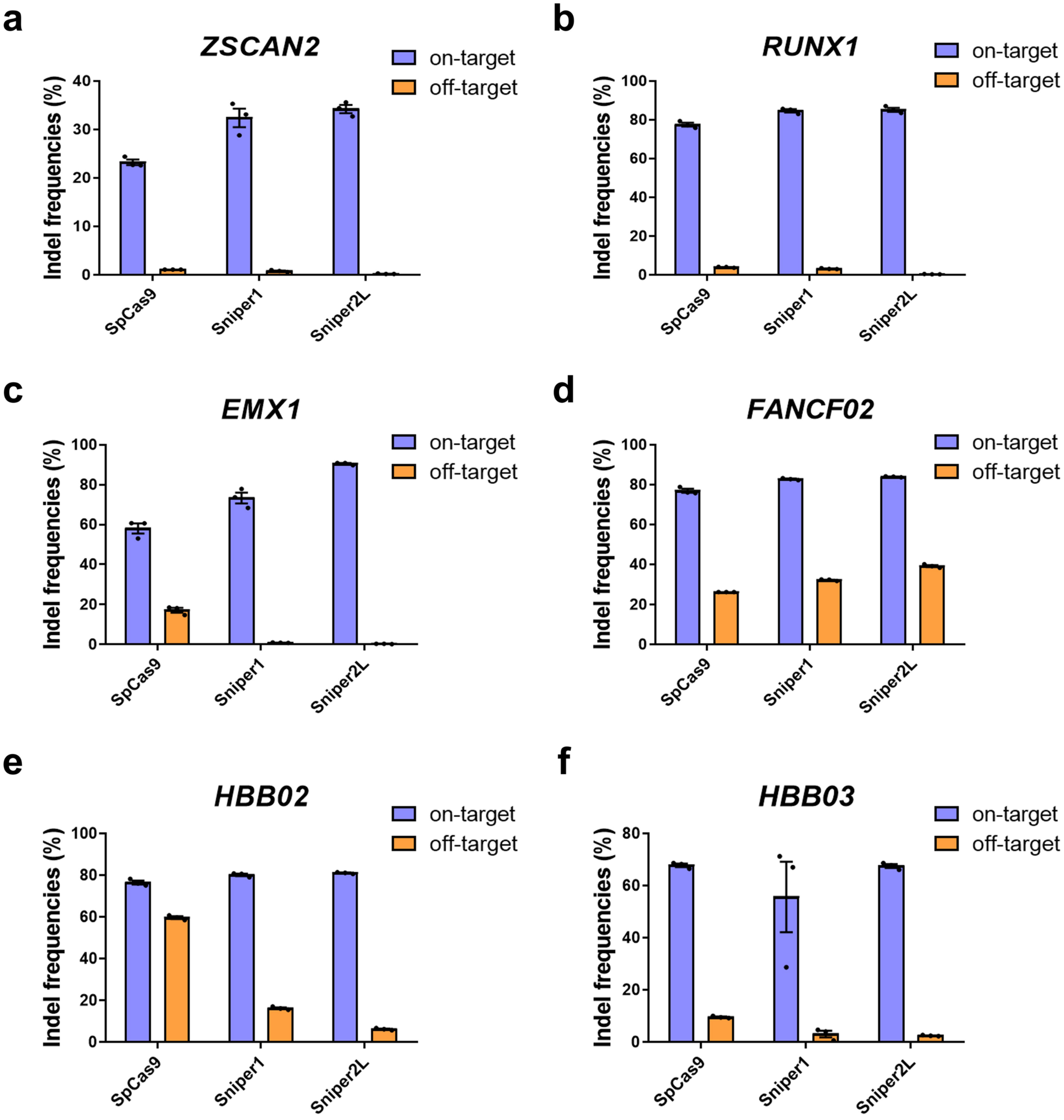

Extended Data Fig. 6 | Indel frequencies induced by RNP delivery of SpCas9, Sniper1, and Sniper2L at on- (blue) and off- (orange) target sequences in HEK293T cells. The name of the gene in which the target sequence is located is indicated at the top of each graph. Error bars indicate s.e.m. The number of independent transfections *n* = 3.

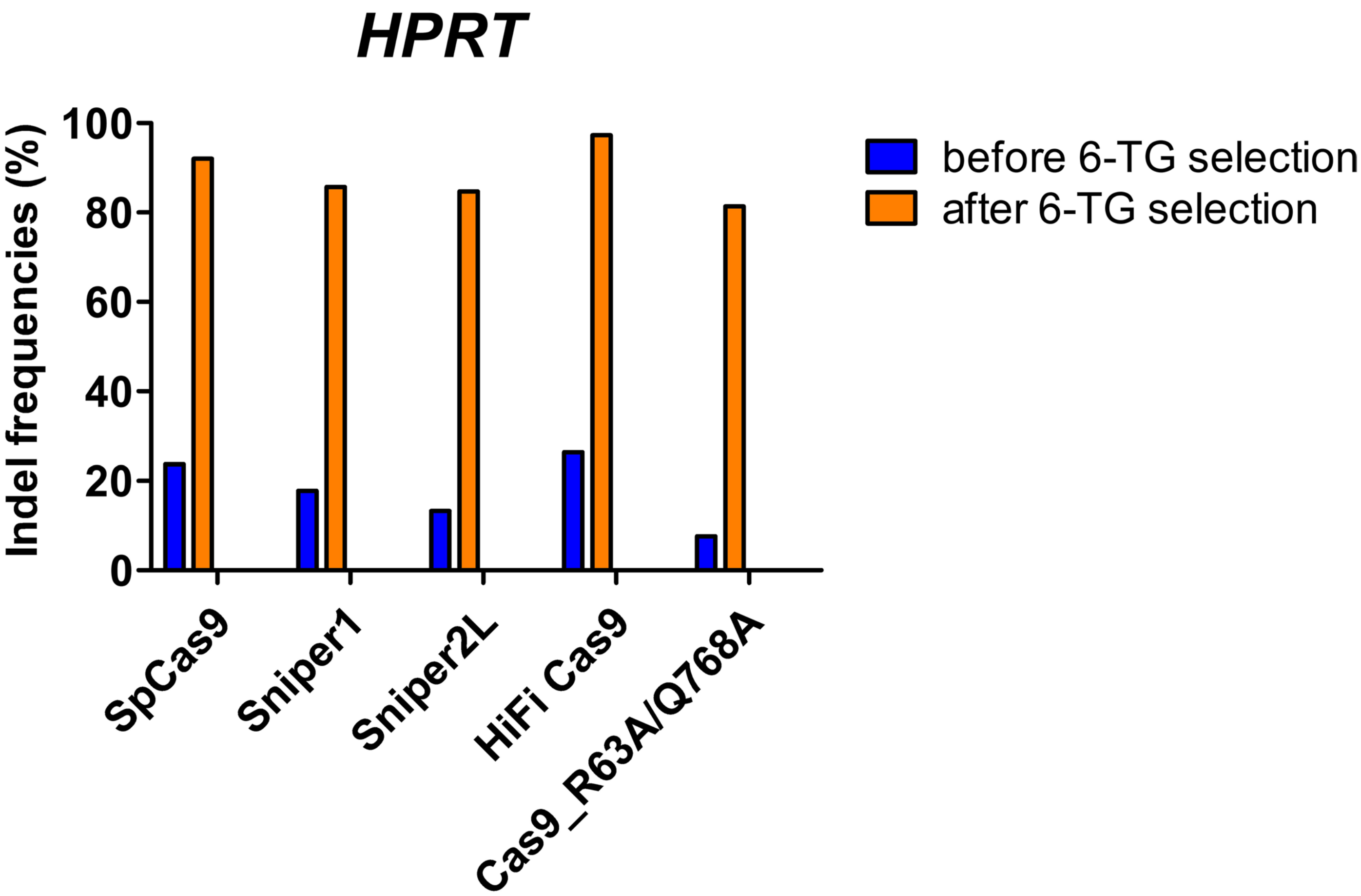

Extended Data Fig. 7 | Enrichment of indel-containing cells by 6-TG. Indel frequencies induced by Cas9 variants in the human *HPRT* gene in the library screen using RNP delivery before and after 6-TG selection.

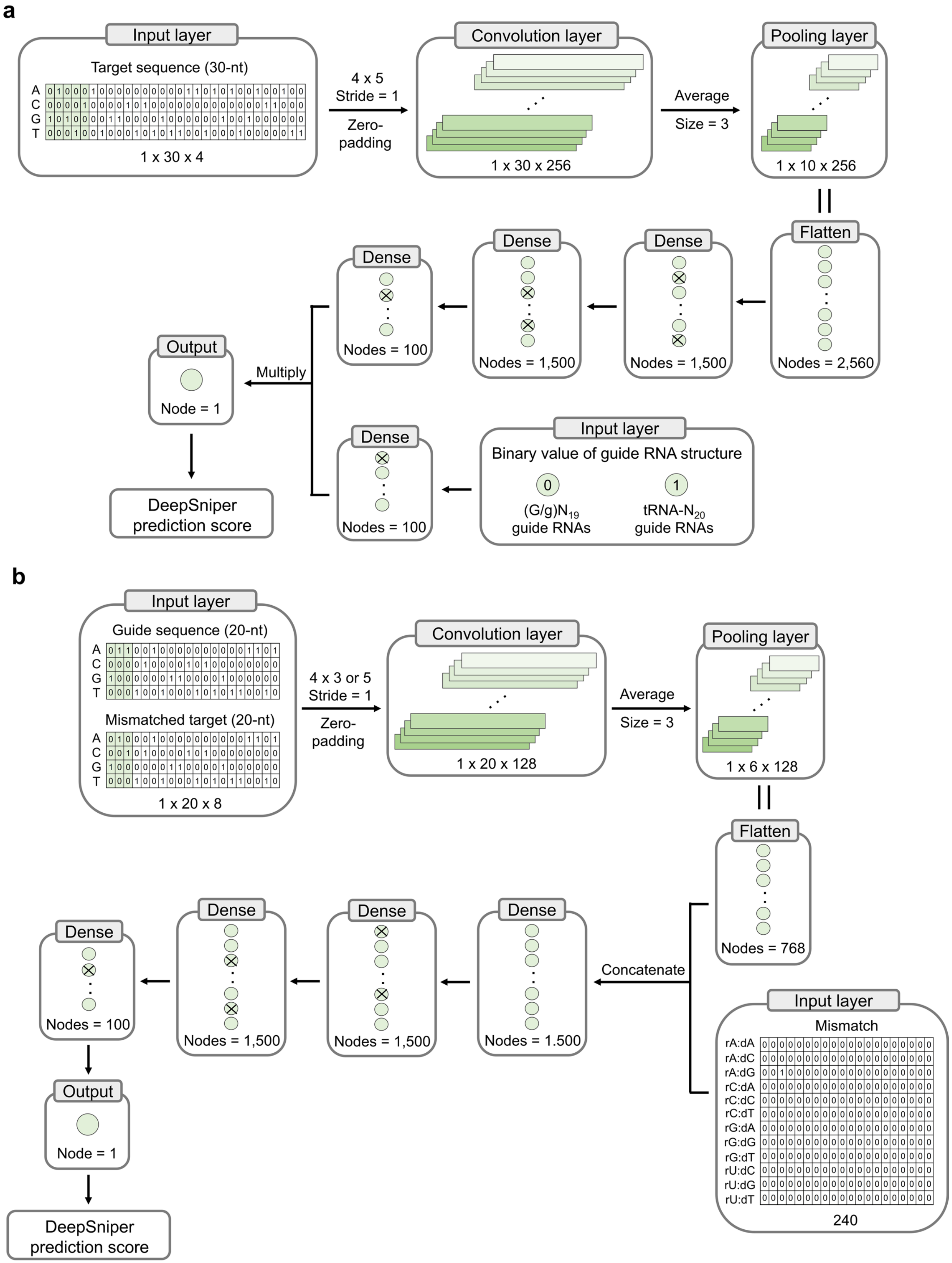

Target sequence (30-nt)

A	0	1	0	0	0	1	0	0	0	0	0	0	0	0	0	0	1	1	0	1	0	1	0	0	1	0	0	1	0	0
C	0	0	0	0	1	0	0	0	0	1	0	1	0	0	0	0	0	0	0	0	0	0	0	0	0	1	1	0	0	0
G	1	0	1	0	0	0	0	1	1	0	0	0	0	1	0	0	0	0	0	0	1	0	0	1	0	0	0	0	0	0
T	0	0	0	1	0	0	1	0	0	0	1	0	1	0	1	1	0	0	1	0	0	0	1	0	0	0	0	0	1	1

Guide sequence (20-nt)

A	0	1	1	0	0	1	0	0	0	0	0	0	0	0	0	0	1	1	0	1
C	0	0	0	0	1	0	0	0	0	1	0	1	0	0	0	0	0	0	0	0
G	1	0	0	0	0	0	0	1	1	0	0	0	0	1	0	0	0	0	0	0
T	0	0	0	1	0	0	1	0	0	0	1	0	1	0	1	1	0	0	1	0

Mismatched target (20-nt)

A	0	1	0	0	0	1	0	0	0	0	0	0	0	0	0	0	1	1	0	1
C	0	0	1	0	1	0	0	0	0	1	0	1	0	0	0	0	0	0	0	0
G	1	0	0	0	0	0	0	1	1	0	0	0	0	1	0	0	0	0	0	0
T	0	0	0	1	0	0	1	0	0	0	1	0	1	0	1	1	0	0	1	0

Mismatch

rA:dA	0	0	0	0	0	0	0	0	0	0	0	0	0	0	0	0	0	0	0	0
rA:dC	0	0	0	0	0	0	0	0	0	0	0	0	0	0	0	0	0	0	0	0
rA:dG	0	0	1	0	0	0	0	0	0	0	0	0	0	0	0	0	0	0	0	0
rC:dA	0	0	0	0	0	0	0	0	0	0	0	0	0	0	0	0	0	0	0	0
rC:dC	0	0	0	0	0	0	0	0	0	0	0	0	0	0	0	0	0	0	0	0
rC:dT	0	0	0	0	0	0	0	0	0	0	0	0	0	0	0	0	0	0	0	0
rG:dA	0	0	0	0	0	0	0	0	0	0	0	0	0	0	0	0	0	0	0	0
rG:dG	0	0	0	0	0	0	0	0	0	0	0	0	0	0	0	0	0	0	0	0
rG:dT	0	0	0	0	0	0	0	0	0	0	0	0	0	0	0	0	0	0	0	0
rU:dC	0	0	0	0	0	0	0	0	0	0	0	0	0	0	0	0	0	0	0	0
rU:dG	0	0	0	0	0	0	0	0	0	0	0	0	0	0	0	0	0	0	0	0
rU:dT	0	0	0	0	0	0	0	0	0	0	0	0	0	0	0	0	0	0	0	0

Extended Data Fig. 8 | Schematic of DeepSniper. Overview of DeepSniper, which predicts the on-target (**a**) and off-target (**b**) activities of Sniper-Cas9 variants.

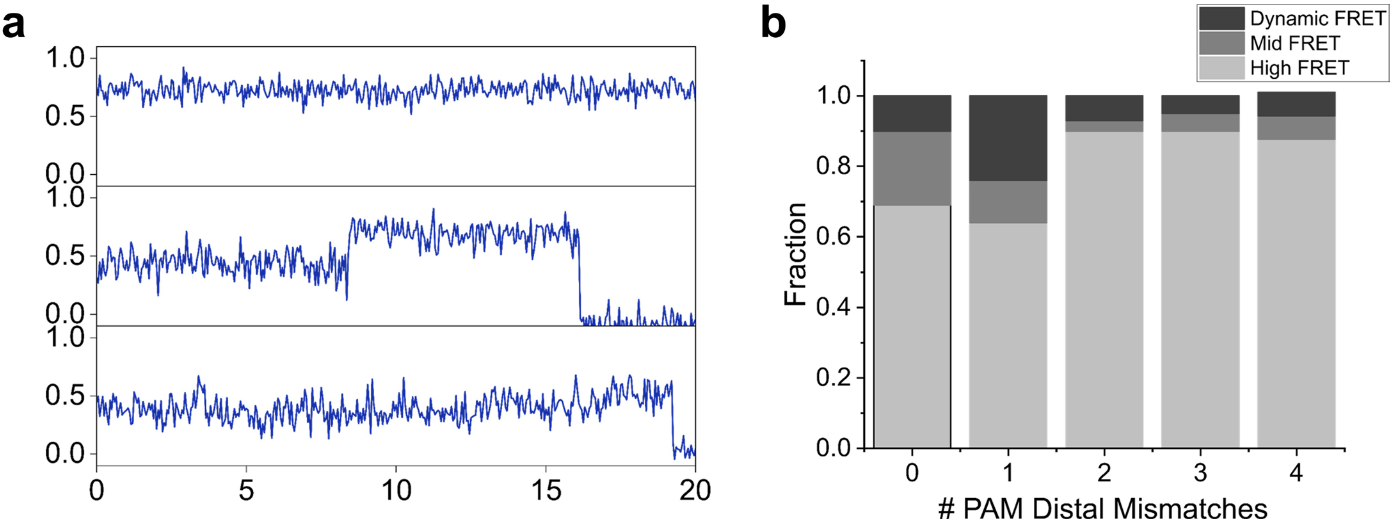

Extended Data Fig. 9 | Transitions between unwound and rewound states are infrequent in FRET experiments. a, Example time traces of FRET efficiency (vertical axis) vs time. An example of constantly high FRET (rewound, top), an example of dynamic FRET, switching between high and mid-level FRET (middle), and an example of constantly mid-level FRET (unwound, bottom) are shown. **b**, Fraction of DNA molecules showing constantly high FRET, dynamic FRET, and constantly mid-level FRET behavior in single-molecule time traces vs. the number of PAM-distal mismatches.

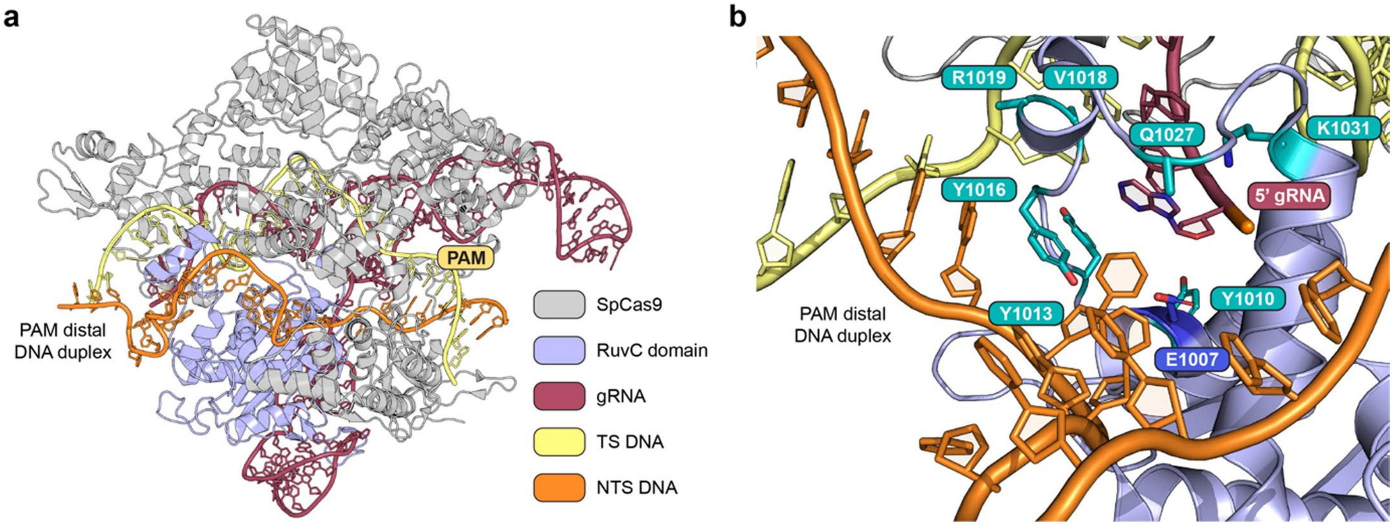

Extended Data Fig. 10 | Structural modeling of SpCas9 residue E1007. (**a**) Structural model of the SpCas9-sgRNA complex bound to a target DNA molecule with a complete target strand (visualized using PDB ID: 5Y36[31]). The proximity between the RuvC domain (light blue) and the reannealing region of the target strand with the non-target strand (NTS) in the PAM distal duplex is shown. This structure was selected for illustrative purposes due to having a complete NTS, despite the 5′GG extension/mismatches; the 5′GG-extension on the gRNA spacer and 13 nt of the PAM distal duplex were omitted from this structure for simplicity. gRNA, guide RNA; TS DNA, target strand DNA; NTS DNA, non-target strand DNA. (**b**) Zoomed in view from above the PAM distal DNA duplex of residue E1007 (show in blue; mutated in Sniper2 variants) in close proximity to the seven amino acid side chains that are substituted in SuperFi-Cas9[28] (visualized using PDB ID: 6VPC[33]). The proximity of the E1007 side chain (in blue) with the 5′ end of the gRNA, along with the SuperFi-Cas9 residues (in teal) and the PAM distal duplex is shown. This ABE8e structure was selected for illustrative purposes because it contained a complete PAM distal end of the R-loop with a canonical 20 nt gRNA spacer; the TadA domains and other structural features unrelated to this visualization were omitted for clarity.

nature research

Corresponding author(s): Jungjoon K. Lee, Taekjip Ha, Hyongbum Henry Kim

Last updated by author(s): Jan 26, 2023

Reporting Summary

Nature Research wishes to improve the reproducibility of the work that we publish. This form provides structure for consistency and transparency in reporting. For further information on Nature Research policies, see our Editorial Policies and the Editorial Policy Checklist.

Statistics

For all statistical analyses, confirm that the following items are present in the figure legend, table legend, main text, or Methods section.

n/a	Confirmed	
□	☒	The exact sample size (*n*) for each experimental group/condition, given as a discrete number and unit of measurement
□	☒	A statement on whether measurements were taken from distinct samples or whether the same sample was measured repeatedly
□	☒	The statistical test(s) used AND whether they are one- or two-sided *Only common tests should be described solely by name; describe more complex techniques in the Methods section.*
□	☒	A description of all covariates tested
□	☒	A description of any assumptions or corrections, such as tests of normality and adjustment for multiple comparisons
□	☒	A full description of the statistical parameters including central tendency (e.g. means) or other basic estimates (e.g. regression coefficient) AND variation (e.g. standard deviation) or associated estimates of uncertainty (e.g. confidence intervals)
□	☒	For null hypothesis testing, the test statistic (e.g. *F*, *t*, *r*) with confidence intervals, effect sizes, degrees of freedom and *P* value noted *Give P values as exact values whenever suitable.*
☒	□	For Bayesian analysis, information on the choice of priors and Markov chain Monte Carlo settings
☒	□	For hierarchical and complex designs, identification of the appropriate level for tests and full reporting of outcomes
□	☒	Estimates of effect sizes (e.g. Cohen's *d*, Pearson's *r*), indicating how they were calculated

Our web collection on statistics for biologists contains articles on many of the points above.

Software and code

Policy information about availability of computer code

Data collection	Illumina Hiseq 2500 and Novaseq was used to collect targeted deep sequencing data.
Data analysis	GraphPad Prism 5 (used only for generating graphs, not for statistical analyses), SPSS Statistics (version 25, IBM), Tensorflow 2.5. Sourcode for DeepSniper and analyzing FRET data are available on github (at https://github.com/NahyeKim/DeepSniper and https://github.com/Ha-SingleMoleculeLab)

For manuscripts utilizing custom algorithms or software that are central to the research but not yet described in published literature, software must be made available to editors and reviewers. We strongly encourage code deposition in a community repository (e.g. GitHub). See the Nature Research guidelines for submitting code & software for further information.

Data

Policy information about availability of data

All manuscripts must include a data availability statement. This statement should provide the following information, where applicable:

- Accession codes, unique identifiers, or web links for publicly available datasets
- A list of figures that have associated raw data
- A description of any restrictions on data availability

We have submitted the deep sequencing data from this study to the NCBI Seqeuence Read Archive under accession number PRJNA817000. We have provided the data sets used in this study as Supplementary Table 2. We used PDB IDs 5Y36 (https://www.rcsb.org/structure/5Y36) and 6VPC (https://www.rcsb.org/structure/6VPC) for structural analyses shown in Extended Data Fig. 10.

Field-specific reporting

Please select the one below that is the best fit for your research. If you are not sure, read the appropriate sections before making your selection.

☒ Life sciences ☐ Behavioural & social sciences ☐ Ecological, evolutionary & environmental sciences

For a reference copy of the document with all sections, see nature.com/documents/nr-reporting-summary-flat.pdf

Life sciences study design

All studies must disclose on these points even when the disclosure is negative.

Sample size

No statistical methods were used to predetermine sample size. Sample sizes were chosen after deep sequencing depending on the number and quality as written in 'Data exclusions'. All sample sizes were sufficient for the following statistical tests (n>3).

Data exclusions

To increase the accuracy of the analysis for indel frequency, deep sequencing data were filtered to exclude target sequences with total deep sequencing read counts, not including reads containing indels, less than 100 or 200. Background indel frequencies which were greater than 8% were also excluded from analyses. These criteria were not pre-established.

Replication

We technically replicated our lentiviral delivery based high-throughput experiments three times for all three variants by a single researcher. All attempts at replication were successful.

Randomization

Mammalian cells utilized in this study were grown under identical conditions. Thus, randomization was not relevant to this study.

Blinding

Mammalian cells utilized in this study were grown under identical conditions. Thus, blinding was not used.

Behavioural & social sciences study design

All studies must disclose on these points even when the disclosure is negative.

Study description

Briefly describe the study type including whether data are quantitative, qualitative, or mixed-methods (e.g. qualitative cross-sectional, quantitative experimental, mixed-methods case study).

Research sample

State the research sample (e.g. Harvard university undergraduates, villagers in rural India) and provide relevant demographic information (e.g. age, sex) and indicate whether the sample is representative. Provide a rationale for the study sample chosen. For studies involving existing datasets, please describe the dataset and source.

Sampling strategy

Describe the sampling procedure (e.g. random, snowball, stratified, convenience). Describe the statistical methods that were used to predetermine sample size OR if no sample-size calculation was performed, describe how sample sizes were chosen and provide a rationale for why these sample sizes are sufficient. For qualitative data, please indicate whether data saturation was considered, and what criteria were used to decide that no further sampling was needed.

Data collection

Provide details about the data collection procedure, including the instruments or devices used to record the data (e.g. pen and paper, computer, eye tracker, video or audio equipment) whether anyone was present besides the participant(s) and the researcher, and whether the researcher was blind to experimental condition and/or the study hypothesis during data collection.

Timing

Indicate the start and stop dates of data collection. If there is a gap between collection periods, state the dates for each sample cohort.

Data exclusions

If no data were excluded from the analyses, state so OR if data were excluded, provide the exact number of exclusions and the rationale behind them, indicating whether exclusion criteria were pre-established.

Non-participation

State how many participants dropped out/declined participation and the reason(s) given OR provide response rate OR state that no participants dropped out/declined participation.

Randomization

If participants were not allocated into experimental groups, state so OR describe how participants were allocated to groups, and if allocation was not random, describe how covariates were controlled.

Ecological, evolutionary & environmental sciences study design

All studies must disclose on these points even when the disclosure is negative.

Study description

Briefly describe the study. For quantitative data include treatment factors and interactions, design structure (e.g. factorial, nested, hierarchical), nature and number of experimental units and replicates.

Research sample

Describe the research sample (e.g. a group of tagged Passer domesticus, all Stenocereus thurberi within Organ Pipe Cactus National

Research sample	*Monument), and provide a rationale for the sample choice. When relevant, describe the organism taxa, source, sex, age range and any manipulations. State what population the sample is meant to represent when applicable. For studies involving existing datasets, describe the data and its source.*
Sampling strategy	*Note the sampling procedure. Describe the statistical methods that were used to predetermine sample size OR if no sample-size calculation was performed, describe how sample sizes were chosen and provide a rationale for why these sample sizes are sufficient.*
Data collection	*Describe the data collection procedure, including who recorded the data and how.*
Timing and spatial scale	*Indicate the start and stop dates of data collection, noting the frequency and periodicity of sampling and providing a rationale for these choices. If there is a gap between collection periods, state the dates for each sample cohort. Specify the spatial scale from which the data are taken*
Data exclusions	*If no data were excluded from the analyses, state so OR if data were excluded, describe the exclusions and the rationale behind them, indicating whether exclusion criteria were pre-established.*
Reproducibility	*Describe the measures taken to verify the reproducibility of experimental findings. For each experiment, note whether any attempts to repeat the experiment failed OR state that all attempts to repeat the experiment were successful.*
Randomization	*Describe how samples/organisms/participants were allocated into groups. If allocation was not random, describe how covariates were controlled. If this is not relevant to your study, explain why.*
Blinding	*Describe the extent of blinding used during data acquisition and analysis. If blinding was not possible, describe why OR explain why blinding was not relevant to your study.*

Did the study involve field work? □ Yes □ No

Field work, collection and transport

Field conditions	*Describe the study conditions for field work, providing relevant parameters (e.g. temperature, rainfall).*
Location	*State the location of the sampling or experiment, providing relevant parameters (e.g. latitude and longitude, elevation, water depth).*
Access & import/export	*Describe the efforts you have made to access habitats and to collect and import/export your samples in a responsible manner and in compliance with local, national and international laws, noting any permits that were obtained (give the name of the issuing authority, the date of issue, and any identifying information).*
Disturbance	*Describe any disturbance caused by the study and how it was minimized.*

Reporting for specific materials, systems and methods

We require information from authors about some types of materials, experimental systems and methods used in many studies. Here, indicate whether each material, system or method listed is relevant to your study. If you are not sure if a list item applies to your research, read the appropriate section before selecting a response.

Materials & experimental systems

n/a	Involved in the study	
□	☒	Antibodies
□	☒	Eukaryotic cell lines
☒	□	Palaeontology and archaeology
☒	□	Animals and other organisms
☒	□	Human research participants
☒	□	Clinical data
☒	□	Dual use research of concern

Methods

n/a	Involved in the study	
☒	□	ChIP-seq
☒	□	Flow cytometry
☒	□	MRI-based neuroimaging

Antibodies

Antibodies used	anti-Cas9 (diluted 1:1000), Biolegend, cat no. 844301 anti-β-actin (diluted 1:1000), Santa Cruz Biotechnology, cat no. sc-47778 horseradish peroxidase-conjugated goat anti-mouse IgG antibody (diluted 1:5000), Santa Cruz Biotechnology, cat no. sc-516102
Validation	https://antibodyregistry.org/search.php?q=AB_2565570 https://antibodyregistry.org/search.php?q=AB_2714189 https://antibodyregistry.org/search.php?q=AB_2687626

Eukaryotic cell lines

Policy information about cell lines

Cell line source(s)

The source of the cell line, HEK293T, is American Type Culture Collection (ATCC).

Authentication

Not been authenticated.

Mycoplasma contamination

Not been tested.

Commonly misidentified lines
(See ICLAC register)

No commonly misidentified cell lines were used.

Palaeontology and Archaeology

Specimen provenance

Provide provenance information for specimens and describe permits that were obtained for the work (including the name of the issuing authority, the date of issue, and any identifying information).

Specimen deposition

Indicate where the specimens have been deposited to permit free access by other researchers.

Dating methods

If new dates are provided, describe how they were obtained (e.g. collection, storage, sample pretreatment and measurement), where they were obtained (i.e. lab name), the calibration program and the protocol for quality assurance OR state that no new dates are provided.

□ Tick this box to confirm that the raw and calibrated dates are available in the paper or in Supplementary Information.

Ethics oversight

Identify the organization(s) that approved or provided guidance on the study protocol, OR state that no ethical approval or guidance was required and explain why not.

Note that full information on the approval of the study protocol must also be provided in the manuscript.

Animals and other organisms

Policy information about studies involving animals; ARRIVE guidelines recommended for reporting animal research

Laboratory animals

For laboratory animals, report species, strain, sex and age OR state that the study did not involve laboratory animals.

Wild animals

Provide details on animals observed in or captured in the field; report species, sex and age where possible. Describe how animals were caught and transported and what happened to captive animals after the study (if killed, explain why and describe method; if released, say where and when) OR state that the study did not involve wild animals.

Field-collected samples

For laboratory work with field-collected samples, describe all relevant parameters such as housing, maintenance, temperature, photoperiod and end-of-experiment protocol OR state that the study did not involve samples collected from the field.

Ethics oversight

Identify the organization(s) that approved or provided guidance on the study protocol, OR state that no ethical approval or guidance was required and explain why not.

Note that full information on the approval of the study protocol must also be provided in the manuscript.

Human research participants

Policy information about studies involving human research participants

Population characteristics

Describe the covariate-relevant population characteristics of the human research participants (e.g. age, gender, genotypic information, past and current diagnosis and treatment categories). If you filled out the behavioural & social sciences study design questions and have nothing to add here, write "See above."

Recruitment

Describe how participants were recruited. Outline any potential self-selection bias or other biases that may be present and how these are likely to impact results.

Ethics oversight

Identify the organization(s) that approved the study protocol.

Note that full information on the approval of the study protocol must also be provided in the manuscript.

Clinical data

Policy information about clinical studies

All manuscripts should comply with the ICMJE guidelines for publication of clinical research and a completed CONSORT checklist must be included with all submissions.

Clinical trial registration

Provide the trial registration number from ClinicalTrials.gov or an equivalent agency.

Study protocol

Note where the full trial protocol can be accessed OR if not available, explain why.

Data collection

Describe the settings and locales of data collection, noting the time periods of recruitment and data collection.

Outcomes

Describe how you pre-defined primary and secondary outcome measures and how you assessed these measures.

Dual use research of concern

Policy information about dual use research of concern

Hazards

Could the accidental, deliberate or reckless misuse of agents or technologies generated in the work, or the application of information presented in the manuscript, pose a threat to:

No	Yes	
□	□	Public health
□	□	National security
□	□	Crops and/or livestock
□	□	Ecosystems
□	□	Any other significant area

Experiments of concern

Does the work involve any of these experiments of concern:

No	Yes	
□	□	Demonstrate how to render a vaccine ineffective
□	□	Confer resistance to therapeutically useful antibiotics or antiviral agents
□	□	Enhance the virulence of a pathogen or render a nonpathogen virulent
□	□	Increase transmissibility of a pathogen
□	□	Alter the host range of a pathogen
□	□	Enable evasion of diagnostic/detection modalities
□	□	Enable the weaponization of a biological agent or toxin
□	□	Any other potentially harmful combination of experiments and agents

ChIP-seq

Data deposition

□ Confirm that both raw and final processed data have been deposited in a public database such as GEO.

□ Confirm that you have deposited or provided access to graph files (e.g. BED files) for the called peaks.

Data access links
May remain private before publication.

For "Initial submission" or "Revised version" documents, provide reviewer access links. For your "Final submission" document, provide a link to the deposited data.

Files in database submission

Provide a list of all files available in the database submission.

Genome browser session
(e.g. UCSC)

Provide a link to an anonymized genome browser session for "Initial submission" and "Revised version" documents only, to enable peer review. Write "no longer applicable" for "Final submission" documents.

Methodology

Replicates

Describe the experimental replicates, specifying number, type and replicate agreement.

Sequencing depth

Describe the sequencing depth for each experiment, providing the total number of reads, uniquely mapped reads, length of reads and whether they were paired- or single-end.

Antibodies

Describe the antibodies used for the ChIP-seq experiments; as applicable, provide supplier name, catalog number, clone name, and lot number.

Peak calling parameters

Specify the command line program and parameters used for read mapping and peak calling, including the ChIP, control and index files used.

Data quality	*Describe the methods used to ensure data quality in full detail, including how many peaks are at FDR 5% and above 5-fold enrichment.*
Software	*Describe the software used to collect and analyze the ChIP-seq data. For custom code that has been deposited into a community repository, provide accession details.*

Flow Cytometry

Plots

Confirm that:

□ The axis labels state the marker and fluorochrome used (e.g. CD4-FITC).

□ The axis scales are clearly visible. Include numbers along axes only for bottom left plot of group (a 'group' is an analysis of identical markers).

□ All plots are contour plots with outliers or pseudocolor plots.

□ A numerical value for number of cells or percentage (with statistics) is provided.

Methodology

Sample preparation	*Describe the sample preparation, detailing the biological source of the cells and any tissue processing steps used.*
Instrument	*Identify the instrument used for data collection, specifying make and model number.*
Software	*Describe the software used to collect and analyze the flow cytometry data. For custom code that has been deposited into a community repository, provide accession details.*
Cell population abundance	*Describe the abundance of the relevant cell populations within post-sort fractions, providing details on the purity of the samples and how it was determined.*
Gating strategy	*Describe the gating strategy used for all relevant experiments, specifying the preliminary FSC/SSC gates of the starting cell population, indicating where boundaries between "positive" and "negative" staining cell populations are defined.*

□ Tick this box to confirm that a figure exemplifying the gating strategy is provided in the Supplementary Information.

Magnetic resonance imaging

Experimental design

Design type	*Indicate task or resting state; event-related or block design.*
Design specifications	*Specify the number of blocks, trials or experimental units per session and/or subject, and specify the length of each trial or block (if trials are blocked) and interval between trials.*
Behavioral performance measures	*State number and/or type of variables recorded (e.g. correct button press, response time) and what statistics were used to establish that the subjects were performing the task as expected (e.g. mean, range, and/or standard deviation across subjects).*

Acquisition

Imaging type(s)	*Specify: functional, structural, diffusion, perfusion.*
Field strength	*Specify in Tesla*
Sequence & imaging parameters	*Specify the pulse sequence type (gradient echo, spin echo, etc.), imaging type (EPI, spiral, etc.), field of view, matrix size, slice thickness, orientation and TE/TR/flip angle.*
Area of acquisition	*State whether a whole brain scan was used OR define the area of acquisition, describing how the region was determined.*

Diffusion MRI □ Used □ Not used

Preprocessing

Preprocessing software	*Provide detail on software version and revision number and on specific parameters (model/functions, brain extraction, segmentation, smoothing kernel size, etc.).*
Normalization	*If data were normalized/standardized, describe the approach(es): specify linear or non-linear and define image types used for transformation OR indicate that data were not normalized and explain rationale for lack of normalization.*
Normalization template	*Describe the template used for normalization/transformation, specifying subject space or group standardized space (e.g.*

Normalization template	*original Talairach, MNI305, ICBM152) OR indicate that the data were not normalized.*
Noise and artifact removal	*Describe your procedure(s) for artifact and structured noise removal, specifying motion parameters, tissue signals and physiological signals (heart rate, respiration).*
Volume censoring	*Define your software and/or method and criteria for volume censoring, and state the extent of such censoring.*

Statistical modeling & inference

Model type and settings	*Specify type (mass univariate, multivariate, RSA, predictive, etc.) and describe essential details of the model at the first and second levels (e.g. fixed, random or mixed effects; drift or auto-correlation).*
Effect(s) tested	*Define precise effect in terms of the task or stimulus conditions instead of psychological concepts and indicate whether ANOVA or factorial designs were used.*

Specify type of analysis: □ Whole brain □ ROI-based □ Both

Statistic type for inference (See Eklund et al. 2016)	*Specify voxel-wise or cluster-wise and report all relevant parameters for cluster-wise methods.*
Correction	*Describe the type of correction and how it is obtained for multiple comparisons (e.g. FWE, FDR, permutation or Monte Carlo).*

Models & analysis

n/a	Involved in the study
□	□ Functional and/or effective connectivity
□	□ Graph analysis
□	□ Multivariate modeling or predictive analysis

Functional and/or effective connectivity	*Report the measures of dependence used and the model details (e.g. Pearson correlation, partial correlation, mutual information).*
Graph analysis	*Report the dependent variable and connectivity measure, specifying weighted graph or binarized graph, subject- or group-level, and the global and/or node summaries used (e.g. clustering coefficient, efficiency, etc.).*
Multivariate modeling and predictive analysis	*Specify independent variables, features extraction and dimension reduction, model, training and evaluation metrics.*